

HEALTH AND MEDICINE

The generation of stable microvessels in ischemia is mediated by endothelial cell derived TRAIL

Siân P. Cartland^{1,2,†}, Manisha S. Patil^{1,2,†}, Elaina Kelland^{1,2}, Natalie Le^{1,2}, Lauren Boccanfuso¹, Christopher P. Stanley^{1,2}, Pradeep Manuneehi Cholan¹, Malathi I. Dona³, Ralph Patrick⁴, Jordan McGrath⁵, Qian Peter Su^{6,7}, Imala Alwis¹, Ruth Ganss⁸, Joseph E. Powell^{9,10}, Richard P. Harvey^{4,11,12}, Alexander R. Pinto³, Thomas S. Griffith¹³, Jacky Loa⁵, Sarah J. Aitken^{2,14,15}, David A. Robinson^{2,5}, Sanjay Patel^{1,5}, Mary M. Kavurma^{1,2,*}

Reversal of ischemia is mediated by neo-angiogenesis requiring endothelial cell (EC) and pericyte interactions to form stable microvascular networks. We describe an unrecognized role for tumor necrosis factor–related apoptosis-inducing ligand (TRAIL) in potentiating neo-angiogenesis and vessel stabilization. We show that the endothelium is a major source of TRAIL in the healthy circulation compromised in peripheral artery disease (PAD). EC deletion of TRAIL in vivo or in vitro inhibited neo-angiogenesis, pericyte recruitment, and vessel stabilization, resulting in reduced lower-limb blood perfusion with ischemia. Activation of the TRAIL receptor (TRAIL-R) restored blood perfusion and stable blood vessel networks in mice. Proof-of-concept studies showed that Conatumumab, an agonistic TRAIL-R2 antibody, promoted vascular sprouts from explanted patient arteries. Single-cell RNA sequencing revealed heparin-binding EGF-like growth factor in mediating EC-pericyte communications dependent on TRAIL. These studies highlight unique TRAIL-dependent mechanisms mediating neo-angiogenesis and vessel stabilization and the potential of repurposing TRAIL-R2 agonists to stimulate stable and functional microvessel networks to treat ischemia in PAD.

INTRODUCTION

Peripheral artery disease (PAD) affects >230 million people worldwide (1). Correcting the ischemia caused by PAD is a key component of current surgical revascularization techniques, but patients still experience disease progression characterized by vessel thrombosis, ulceration, and gangrene. These complications of severe PAD often necessitate surgical amputation of limbs. Alarming, by 2050, >3.5 million US citizens are expected to live without a limb (2). Surgical revascularization and amputation merely address the immediate complications of PAD while the underlying disease processes continue to place patients at risk of further adverse limb and cardiovascular outcomes.

One therapeutic approach is to stimulate angiogenesis and bypass the arterial occlusion, restoring the nutrient supply necessary for tissue survival. “Therapeutic angiogenesis” has been studied experimentally but attempts to achieve this in people using angiogenic factors such as vascular endothelial growth factor (VEGF) have failed (3). These treatments did not adequately maintain stability of the newly formed endothelial cell (EC) vessels, which were underdeveloped,

disorganized, and leaky, like those observed in tumor vasculature (4). To generate functional microvessel networks in ischemia, pericyte investment is essential, but processes mediating angiogenesis and EC-pericyte cross-talk are not fully understood. Microvessel development and function is disrupted in cardiovascular diseases, and this limitation has driven the need to better understand processes mediating blood vessel formation and stabilization in ischemia.

Tumor necrosis factor–related apoptosis-inducing ligand (TRAIL) was discovered almost 30 years ago for its unique ability to selectively kill human cancer cells upon binding to its apoptosis-inducing receptors, TRAIL-R1 and TRAIL-R2 [also known as death receptors 4 and 5; (DR4 and DR5, respectively)]. TRAIL-mediated signaling in mice is similar except that only one signaling receptor exists at the protein level, TRAIL-R (also DR5). In contrast to the canonical apoptosis-inducing function of TRAIL, we identified alternate non-apoptotic functions in the vasculature (5–13). Using a mouse model of PAD, *Trail*^{−/−} mice developed limb necrosis associating with a marked reduction in vascularization and blood perfusion (11). We and others have shown that exogenous TRAIL administration stimulated angiogenic processes in vitro and in vivo (11, 14, 15). Whether TRAIL can stimulate stable microvasculature in PAD is unknown.

We have discovered that EC-derived TRAIL modulates EC-pericyte interactions for effective microvessel function so that stable blood vessel networks are created. We identified that ECs are a major contributor of circulating TRAIL levels, compromised in patients with PAD, and associating with reduced numbers of stable microvessels in ischemic amputated tissues. Activation of TRAIL-R restored blood perfusion, vascularization, and vessel stabilization in mice. Proof-of-concept studies showed that Conatumumab, a human agonistic TRAIL-R2 monoclonal antibody (mAb) used in cancer therapy (16), stimulated angiogenic sprouts ex vivo in vessels isolated from patients with PAD. Together, these data suggest that TRAIL-R2 agonist therapy could be a feasible means to increase

¹Heart Research Institute, The University of Sydney, Sydney, Australia. ²Centre for Peripheral Artery Disease, Heart Research Institute, Sydney, Australia. ³Baker Heart and Diabetes Institute, Melbourne, Australia. ⁴Victor Chang Cardiac Research Institute, Sydney, Australia. ⁵Royal Prince Alfred Hospital, Sydney, Australia. ⁶School of Biomedical Engineering, University of Technology, Sydney, Australia. ⁷Heart Research Institute, Sydney, Australia. ⁸Harry Perkins Institute of Medical Research, The University of Western Australia, Perth, Australia. ⁹Garvan-Weizmann Centre for Cellular Genomics, Sydney, Australia. ¹⁰UNSW Cellular Genomics Futures Institute, University of New South Wales, Sydney, Australia. ¹¹School of Clinical Medicine, Faculty of Medicine and Health, University of New South Wales, Sydney, Australia. ¹²School of Biotechnology and Biomolecular Sciences, Faculty of Science, University of New South Wales, Sydney, Australia. ¹³University of Minnesota, Minneapolis, MN 55455, USA. ¹⁴Faculty of Medicine and Health, The University of Sydney, Sydney, Australia. ¹⁵Concord Institute of Academic Surgery, Concord Hospital, Sydney, Australia.

*Corresponding author. Email: mary.kavurma@hri.org.au

†These authors contributed equally to this work.

limb perfusion by improving blood vessel function and promoting stable microvascular networks, a potentially life-changing outcome for these patients.

RESULTS

TRAIL and TRAIL-R2 expression and interaction are augmented in 24-hour hypoxia in ECs

The impact of hypoxia on TRAIL or TRAIL receptor gene expression in ECs is unclear. To examine this, human microvascular EC-1

(HMEC-1) were exposed to hypoxic (2% O₂) or normoxic conditions over 24 hours. *Trail* and *Trail-R2* mRNA was ~2- and ~1.5-fold higher after the induction of hypoxia, with no changes to *Trail-R1* mRNA (Fig. 1A and fig. S1). TRAIL and TRAIL-R2 surface protein expression was also amplified with 24-hour hypoxia, with no change in total TRAIL-R1 protein expression (Fig. 1, B to D). TRAIL physically interacted with TRAIL-R2 but not TRAIL-R1 under normal conditions, and this interaction was further augmented with hypoxia (Fig. 1E). These results indicate that TRAIL–TRAIL-R2 signaling may be relevant in PAD.

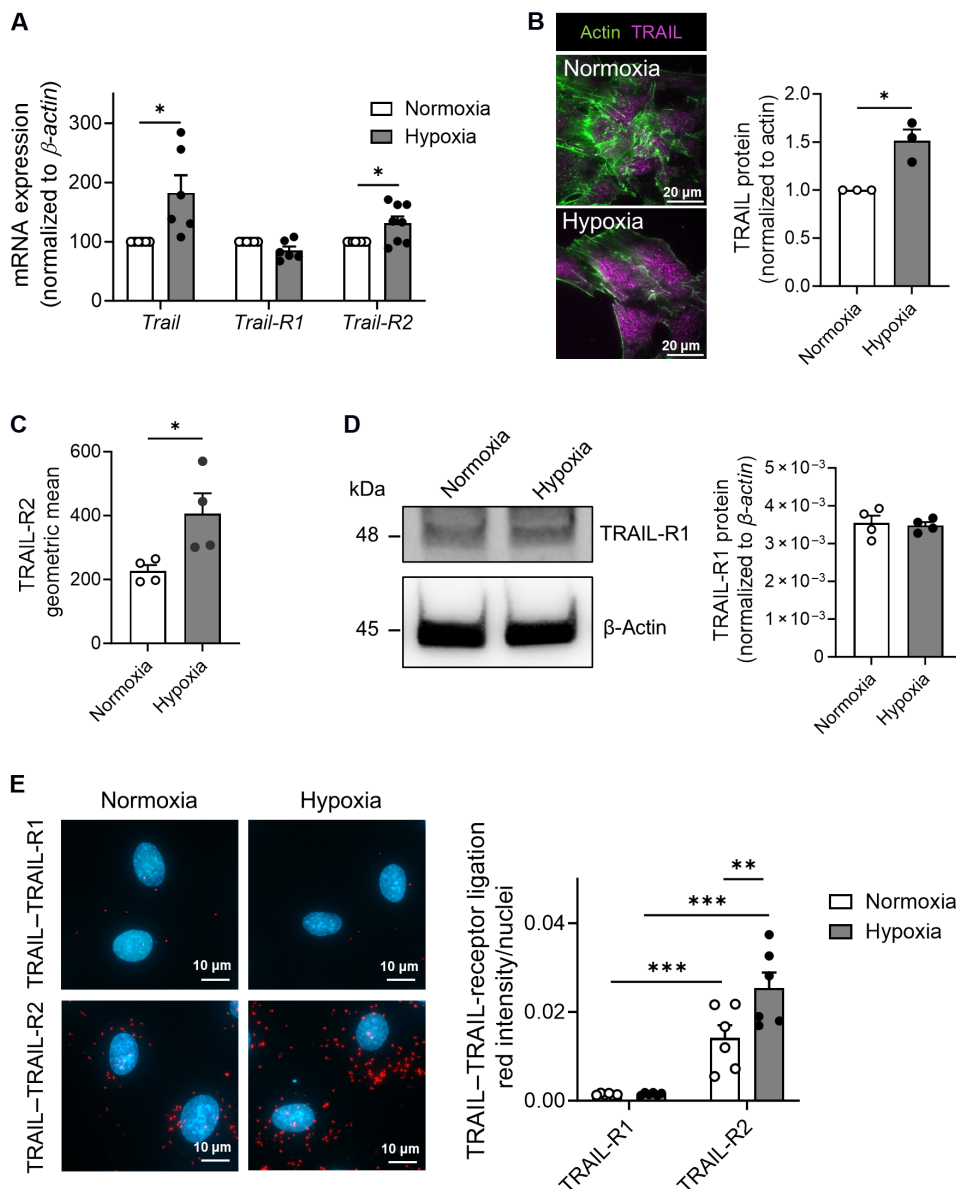


Fig. 1. TRAIL and TRAIL-R2 expression and interaction are augmented in hypoxia. (A) *Trail*, *Trail-R1*, and *Trail-R2* mRNA expression in HMEC-1 after exposure to hypoxia (2% O₂) or normoxia (21% O₂) for 24 hours, qPCR normalized to β -actin ($n = 6$ to 8 per treatment). (B) Total internal reflection fluorescence microscopy images (left) and quantification (right) of TRAIL cell surface expression ($n = 3$ per treatment). (C) TRAIL-R2 cell surface expression by flow cytometry ($n = 4$ per treatment). (D) Left: Western blot of TRAIL-R1 and β -actin. Right: TRAIL-R1 protein expression normalized to β -actin ($n = 4$ per group). (E) Protein-protein interactions between TRAIL–TRAIL-R1 and TRAIL–TRAIL-R2, measured using the Duolink Proximity Ligation Assay. Interactions are indicated by red staining. Left: Representative image. Right: Quantification ($n = 6$ per treatment). Results are means \pm SEM; Student's t test or two-way analysis of variance (ANOVA); * $P < 0.05$, ** $P < 0.01$, and *** $P < 0.001$.

Reduced plasma TRAIL levels in patients associate with reduced numbers of stable microvessels with ischemia

We collected plasma from 11 patients with PAD and found that circulating TRAIL levels were markedly reduced compared to those in 12 healthy individuals, whereas TRAIL-R2 levels were increased (Fig. 2, A and B, and table S1). Muscle tissues were collected following below-knee amputation, and ischemic tissues had lower stable microvessel numbers ($CD31^+SMA^+$ vessels < 50 μm in diameter, arrows) (Fig. 2, C and D), associating with impaired endothelial-dependent vasodilation (Fig. 2E). Single-cell RNA sequencing (scRNA-seq) of mononuclear

cells from nonischemic and ischemic muscle tissue from a patient identified four EC (EC1 to EC4) populations (fig. S2, A and B). scRNA-seq revealed the endothelium as a substantial source of TRAIL, and its expression reduced with ischemia (fig. S2, C and D, and Fig. 2F); ischemia was verified by ~3.5-fold increased *Hif1 α* mRNA (fig. S2E). *Trail* mRNA was also suppressed in ischemic limbs of wild-type mice after hindlimb ischemia (HLI), our preclinical model of PAD, associating with reduced blood perfusion to the limbs (fig. S2, F and G). Moreover, hypoxia-inducible *Trail* mRNA expression was no longer evident in HMEC-1 at 7 days (fig. S2H). Because

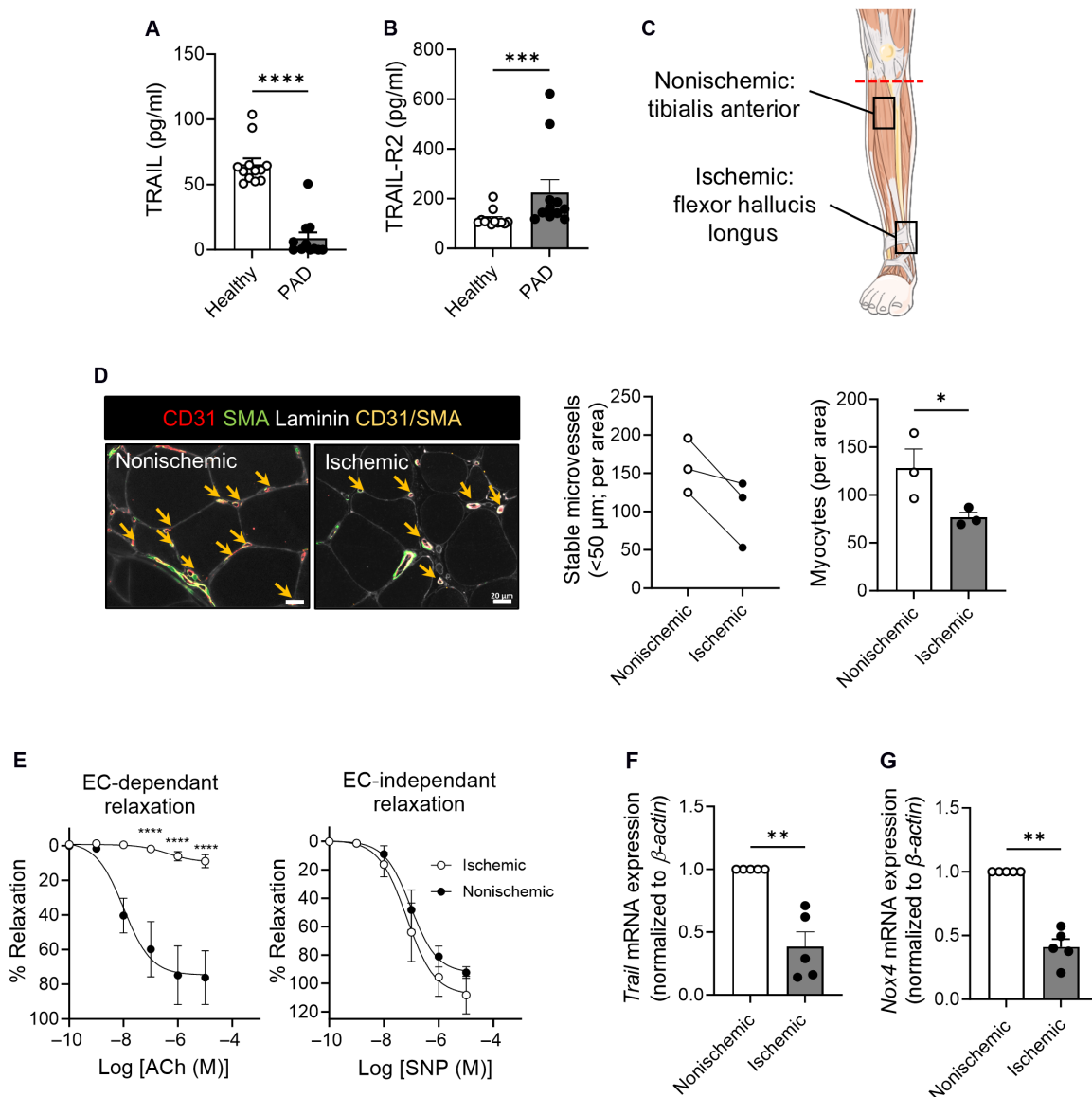


Fig. 2. Plasma TRAIL levels are reduced in PAD, associating with reduced microvessel numbers with increasing ischemia. Plasma (A) TRAIL and (B) TRAIL-R2 levels in PAD versus healthy individuals ($n = 11$ to 12 per group). (C) Schematic illustrating tissue harvest locations from below-knee amputations. (D) Stable microvessel numbers in nonischemic and ischemic regions of amputated tissues. Left: Representative image of stable microvessels ($CD31^+SMA^+$, yellow arrows). Laminin (myocytes, white), CD31 (ECs, red), and SMA (pericytes, green); scale bars, $20 \mu\text{m}$. Middle: Microvessel quantification. Right: Myocyte number is reduced with ischemia ($n = 3$ per group). (E) Myography showing impaired endothelial function in arteries isolated from nonischemic versus ischemic regions. Left: Arterial relaxation in response to increasing doses of acetylcholine (ACh). Right: No change in sodium nitroprusside (SNP)-mediated relaxation ($n = 5$ per group). (F) *Trail* and (G) *Nox4* mRNA expression in patient tissues ($n = 5$ per group). mRNA normalized to β -actin. Results are means \pm SEM; Mann-Whitney *U* test, paired *t* test, or two-way ANOVA; * $P < 0.05$, ** $P < 0.01$, *** $P < 0.001$, and **** $P < 0.0001$.

NADPH oxidase-4 (NOX4) is downstream of TRAIL and is critical for endothelial function and angiogenesis in lower extremity ischemia (11, 17). *Nox4* mRNA was measured, and its expression was also reduced with ischemia in patient limbs (Fig. 2G). Thus, under chronic conditions of ischemia or hypoxia, suppression of TRAIL may compromise EC function(s) including processes of angiogenesis and vessel stabilization.

ECs are a major cellular and circulating source of TRAIL in mice

To examine the contribution of EC-derived TRAIL to angiogenesis and vessel stabilization, we generated EC-specific *Trail*^{-/-} (*Trail*^{EC-/-}) mice. Quantitative polymerase chain reaction (qPCR) analysis of the CD31⁺ EC population isolated from *Trail*^{EC-/-} lung and brain confirmed deletion of *Trail* mRNA, but not of its receptor, *Trail-R* (fig. S3, A and B). In contrast, *Trail* and *Trail-R* mRNA levels were unaltered in vascular smooth muscle cell-rich aortae between each genotype (fig. S3C). We examined aortae of adult *Trail*^{EC-/-} and *Trail*^{EC+/+} mice to assess whether EC-specific TRAIL deletion affected large vessel architecture. No change in media area was observed, nor there were differences in collagen or elastin content (fig. S3D). The absence of TRAIL in the endothelium did not affect plasma cholesterol, insulin, or glucose levels, but plasma TRAIL levels were reduced in *Trail*^{EC-/-} by ~60% (table S2), indicating that ECs are a major source of TRAIL in the circulation.

EC-derived TRAIL stimulates neo-angiogenesis and pericyte recruitment and wrapping

Pericyte investment is critical to forming healthy and sustainable vasculature, which stabilizes and matures nascent blood vessels. Without proper acquisition and pericyte coverage, EC microvascular functions are compromised. For example, reduced EC-pericyte association results in vascular leak and impaired blood flow (18). We found significantly more leakage (~2-fold) into highly vascularized organs of *Trail*^{EC-/-} mice (Fig. 3A). We next examined the contribution of EC-derived TRAIL to facilitate blood vessel formation using the Matrigel plug assay as a model of angiogenesis. Capillary density and perivascular cell content in plugs from *Trail*^{EC-/-} were ~60 and 50% less than in plugs from *Trail*^{EC+/+} mice (Fig. 3, B and C, arrows). Because pericytes are defined by ≥2 markers, we assessed the most common, NG2 (neural/glial antigen 2), RGS5 (regulator of G protein signaling 5), and PDGFRβ (platelet-derived growth factor receptor-β) and found ~50% reduction in mRNA of each within the plug (Fig. 3D). In vitro, *Trail*^{+/+} ECs formed ~50% more tubules than *Trail*^{-/-} ECs at 6 hours, dissociating by 24 hours (Fig. 3E and fig. S4A). Primary pericytes also had a threefold increased capacity to migrate to *Trail*^{+/+} but not *Trail*^{-/-} ECs (Fig. 3F). Further, physiological doses of recombinant TRAIL stimulated primary pericyte proliferation and migration but not of a pericyte precursor cell line, 10 T1/2, suggesting that TRAIL may be responsible for recruitment and proliferation of mature pericytes (fig. S4, B to E). Exposure of pericytes to *Trail*^{+/+} but not *Trail*^{-/-} EC tubules prolonged their survival to 24 hours (Fig. 3G). These confirm that TRAIL-expressing ECs are important for angiogenesis, pericyte recruitment, and wrapping, which is necessary for vessel stabilization.

Trail^{EC-/-} mice have impaired microvascular networks in ischemia

HLI causes major ischemia in skeletal muscle of limbs. *Trail*^{EC-/-} gastrocnemius tissues had a significant reduction in stable microvessels

3 days after HLI and remained reduced at day 28 (Fig. 4, A and B; CD31⁺SMA⁺ < 50 μm in diameter, arrows), associating with reduced blood perfusion over time (Fig. 4C). There was no change in larger vessel numbers (fig. S5A). Consistent with reduced pericyte investment, a ~50% reduction in *Ng2* and *Pdgfrβ* but not *Rgs5* mRNA was observed in ischemic tissues of *Trail*^{EC-/-} mice at day 3 (Fig. 4D). Furthermore, *Trail*^{EC-/-} aortic explants exposed to hypoxia exhibited diminished sprout numbers and sprout length (Fig. 4, E to G).

scRNA-seq identifies altered gene expression profiles with ischemia in *Trail*^{EC-/-} mice

To examine the molecular determinants of EC processes dependent on TRAIL signaling, we performed scRNA-seq of mononuclear cells isolated from control and ischemic tissues of *Trail*^{EC-/-} and *Trail*^{EC+/+} mice 3 days after HLI, where stable microvessel numbers and pericyte marker expression are reduced (Fig. 4, A and D). Unlike the human setting, mice presented with seven EC (EC1 to EC7) and one lymphatic EC (LEC) subtypes (fig. S6, A to C). We identified 3636 differentially expressed genes (DEGs) in the EC1 to EC7 populations. Interrogation of these in ischemic *Trail*^{EC+/+} tissues showed enrichment for positive adenosine 5'-triphosphate synthesis and metabolic processes, translation, mitochondrial organization, and aerobic respiration, findings not observed in *Trail*^{EC-/-} ischemic limbs (fig. S7, A to C and tables S4 and S5).

We next examined TRAIL expression and found that it was enriched in all EC populations in *Trail*^{EC+/+} mice (fig. S6, D and E). In response to ischemia, TRAIL expression was reduced in EC5, EC7, EC1, EC2, EC4, and LEC by 67.8, 62.9, 40.7, 22.0, 22.8, and 13.6%, respectively (fig. S6E). We could not assess TRAIL expression in EC6 as this group was completely absent after ischemia (fig. S6B). In contrast, EC3 showed increased TRAIL expression by 38%, implying that this microvessel population could contribute to TRAIL's beneficial effects in ischemia (fig. S6, E and F, and table S3). Inspection of the up-regulated DEGs within this EC subtype identified many pro-angiogenic genes (Table 1).

TRAIL signals facilitate EC-pericyte communication

We next assessed EC-to-pericyte communications using CellChat (19). Multiple signals were enriched in the EC1 to EC7 population when comparing control versus ischemic *Trail*^{EC+/+} limbs, including the most studied EC-pericyte signal, PDGFRβ-to-PDGFRβ (fig. S8A). When we directly compared EC-pericyte signals in ischemic limbs between genotype, many pathways were altered (fig. S8B). Of interest, heparin-binding EGF-like growth factor (HBEGF) signals were absent in *Trail*^{EC-/-} ischemic limbs (fig. S8B, arrows). HBEGF is known to regulate pericyte recruitment via its receptors EGFR and ERBB2 (20–22). Notably, TRAIL was reported to increase HBEGF transcription in ECs (23), suggesting that this pathway may be important. Validation studies confirmed ~50% reduction in *Hbegf* in *Trail*^{-/-} versus *Trail*^{+/+} ECs, whereas the negative control *Lamc1* mRNA was unchanged (Fig. 5A). *Erb2* mRNA was reduced in *Trail*^{EC-/-} limb tissues, with no changes to *Egfr* (Fig. 5B). HBEGF receptors were also expressed in primary pericytes (Fig. 5C). Human ischemic versus nonischemic muscle showed reduced mRNA expression for *Hbegf* and *Erb2* but not *Egfr* (Fig. 5D). We examined the TRAIL-HBEGF link further; administration of recombinant HBEGF to *Trail*^{EC-/-} gastrocnemius increased stable blood vessel numbers and improved blood reperfusion 14 days after HLI (Fig. 5, E and F). This was, in part, through increased expression and

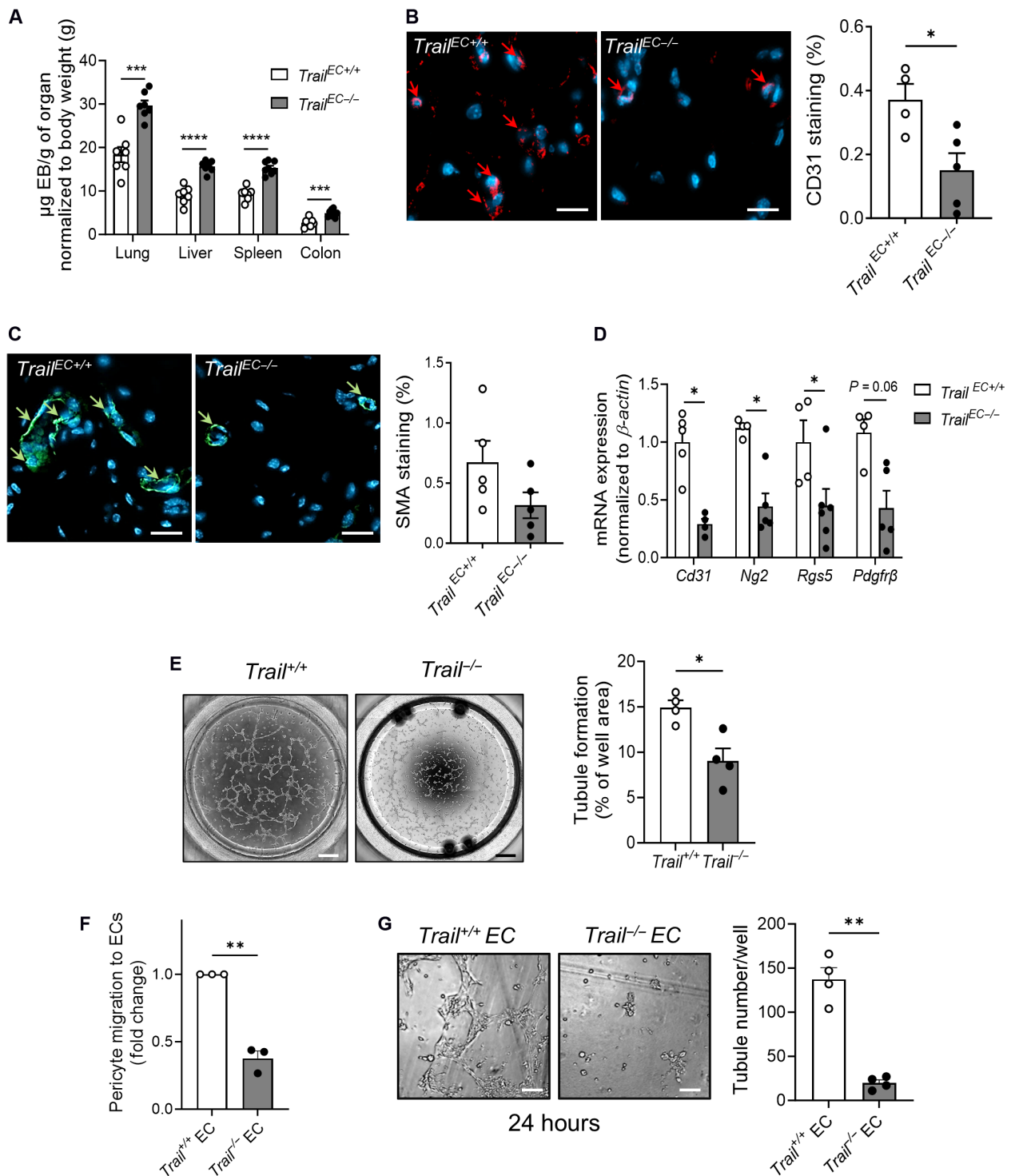


Fig. 3. EC-derived TRAIL regulates neo-angiogenesis, pericyte recruitment, and vessel stabilization. (A) Permeability of Evans Blue (EB) into highly vascularized organs from *Trail*^{EC+/+} and *Trail*^{EC-/-} mice ($n = 7$ to 8 per group). *Trail*^{EC+/+} and *Trail*^{EC-/-} mice were injected with Matrigel; plugs were collected 28 days later and (B) capillary density (CD31, red) and (C) perivascular cell (SMA, green) content determined by microscopy; scale bars, $20\ \mu\text{m}$ ($n = 4$ to 5 per group). (D) EC and pericyte mRNA marker expression in Matrigel plugs was measured by qPCR, normalized to β -actin ($n = 4$ to 5 per group). (E) Tubule formation in *Trail*^{+/+} and *Trail*^{-/-} ECs at 6 hours. Left: Representative images; scale bars, $500\ \mu\text{m}$. Right: Quantification ($n = 4$ per group). (F) Pericyte migration to *Trail*^{+/+} and *Trail*^{-/-} ECs by Transwell assay at 8 hours ($n = 3$ per group). (G) Increased tubule numbers at 24 hours in *Trail*^{+/+} but not *Trail*^{-/-} ECs cocultured with pericytes. Left: Representative images; scale bars, $100\ \mu\text{m}$. Right: Quantification. ECs and pericytes isolated from mouse brain. Results are means \pm SEM; Student's t test, paired t test, or Mann-Whitney U test; * $P < 0.05$, ** $P < 0.01$, *** $P < 0.001$, and **** $P < 0.001$.

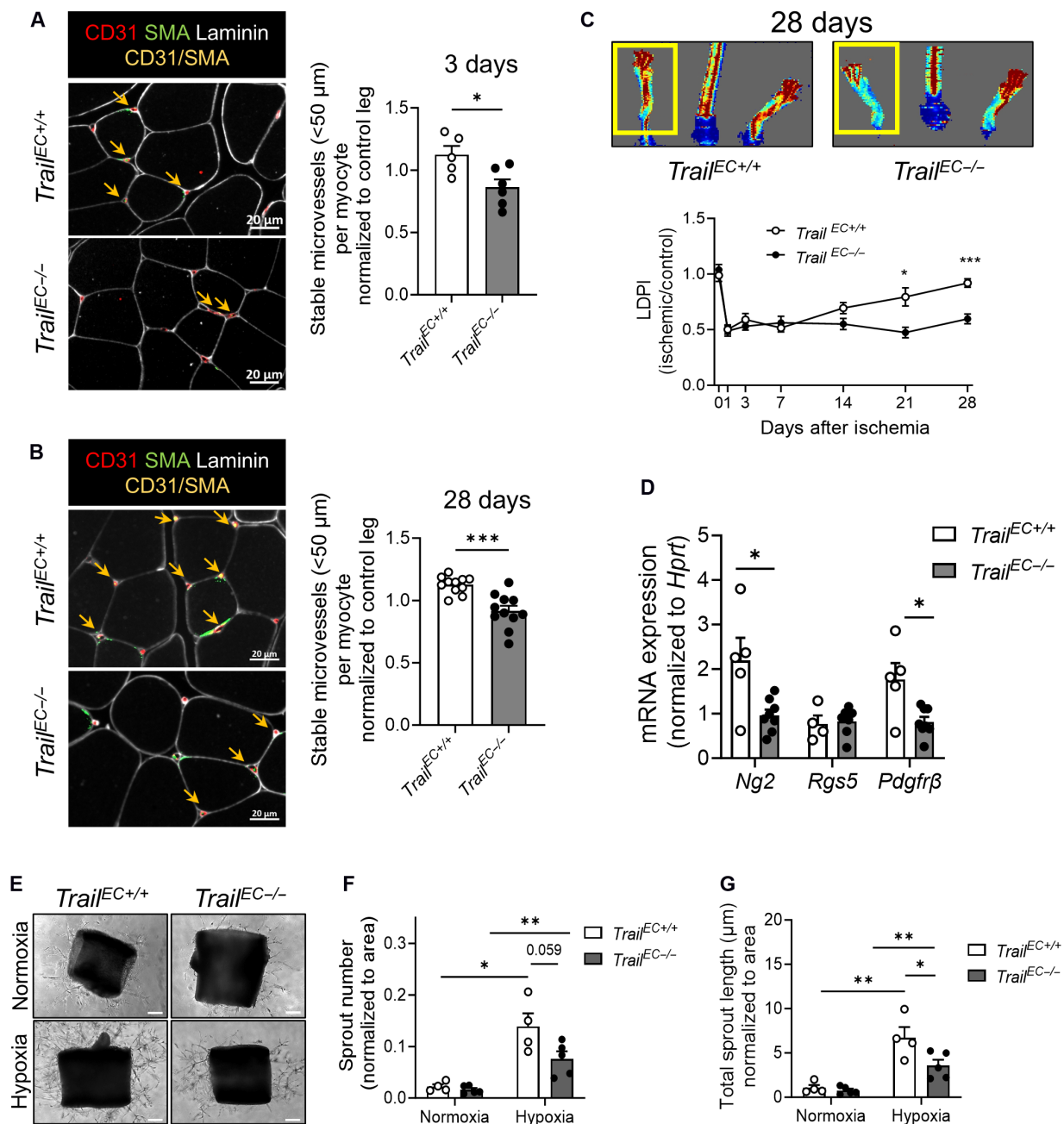


Fig. 4. Stable microvessel numbers are reduced in ischemic limb tissues of *Trail*^{EC-/-} mice. (A) Stable microvessels (CD31⁺SMA⁺; yellow arrows) in gastrocnemius muscle of *Trail*^{EC+/+} and *Trail*^{EC-/-} mice 3 days after HLI. Left: Representative image of ischemic muscle stained for laminin, CD31, and SMA; scale bars, 20 μm . Right: Quantification ($n = 5$ to 6 per genotype). (B) Stable microvessels (CD31⁺SMA⁺; yellow arrows) in gastrocnemius muscle of *Trail*^{EC+/+} and *Trail*^{EC-/-} 28 days after HLI. Left: Representative image of ischemic muscle stained for laminin, CD31, and SMA; scale bars, 20 μm . Right: Quantification ($n = 11$ per genotype). (C) Laser Doppler imaging showing blood perfusion over time in *Trail*^{EC+/+} and *Trail*^{EC-/-} mice after HLI. Top: Representative image of blood flow at 28 days. Bottom: Quantification over time ($n = 9$ to 11 mice per genotype). (D) Pericyte marker mRNA expression in ischemic limbs of *Trail*^{EC+/+} and *Trail*^{EC-/-} mice 3 days after HLI, normalized to hypoxanthine-guanine phosphoribosyl transferase, *Hprt* ($n = 4$ to 8 per group). All data from (A) to (D) were normalized to the respective nonischemic control limb. (E) Representative sprouting images. Aortae from *Trail*^{EC+/+} and *Trail*^{EC-/-} mice in response to 8-day hypoxia (2% O₂) ex vivo; scale bars, 100 μm . Quantification of (F) sprout number and (G) total sprout length ($n = 4$ to 5 per genotype). Results are means \pm SEM; Mann-Whitney *U* test or two-way ANOVA; * $P < 0.05$, ** $P < 0.01$, and *** $P < 0.001$.

Table 1. Top 20 up-regulated genes in response to ischemia in EC3. NADH, reduced form of nicotinamide adenine dinucleotide (oxidized form); IL-6, interleukin-6; Stat6, signal transducer and activator of transcription 6; PI3K, phosphatidylinositol 3-kinase; mTOR, mammalian target of rapamycin.

Gene	Log ₂ fold change	Adjusted P value	Function	Ref
<i>Ndufb11</i>	1.23	1.14×10^{-11}	Mitochondrial complex 1 protein	
<i>Ppp1r14b</i>	1.14	0.022004177	Involved in tumor growth, invasion, and metastasis	(55)
<i>Hbb-bs</i>	1.09	0.000483603	Regulates nitric oxide signaling in ECs	(56)
<i>Atp5d</i>	1.06	3.17×10^{-8}	Subunit of mitochondrial ATP synthase	(57)
<i>D8Ertd738e</i>	1.06	0.004163821	Hypothetical protein	
<i>Atp5g1</i>	1.02	0.008927662	Subunit of mitochondrial ATP synthase	
<i>Ubb</i>	0.98	2.22×10^{-27}	Antiangiogenic	(58)
<i>Ndufb9</i>	0.97	1.27×10^{-7}	Accessory subunit mitochondrial membrane respiratory chain NADH dehydrogenase	
<i>AY036118</i>	0.97	1.47×10^{-31}	Hypothetical protein	
<i>Ifi27</i>	0.97	0.001347498	Increases angiogenesis and tumour growth	(59)
<i>Fabp5</i>	0.96	5.97×10^{-5}	Promotes tumor angiogenesis through IL-6/Stat6/VEGF	(60)
<i>Eef1d</i>	0.96	7.48×10^{-8}	Up-regulated in osteosarcoma; stimulates tumor growth	(61)
<i>Cmss1</i>	0.94	1.14×10^{-46}	Promotes tumor angiogenesis by activating PI3K/Akt/mTOR	(62)
<i>Atp5o</i>	0.93	0.001164086	Subunit of mitochondrial ATP synthase	
<i>Snrpb</i>	0.92	0.000293218	Oncogene	(63)
<i>Ndufb7</i>	0.92	2.44×10^{-6}	Mitochondrial complex 1 subunit	
<i>Nenf</i>	0.90	0.002421906	Up-regulated in ischemia and improves EC function	(64)
<i>Edf1</i>	0.90	2.13×10^{-6}	Regulates EC differentiation	(65)
<i>Ctsz</i>	0.88	6.49×10^{-6}	Stimulates angiogenesis	(66)
<i>Pkm</i>	0.87	0.042740906	Involved in glycolysis	

phosphorylation of endothelial nitric oxide synthase (eNOS) (Fig. 5G). These findings highlight the TRAIL-HBEGF axis in mediating EC-pericyte communications necessary for stable microvessel formation in ischemia.

TRAIL-R activation stimulates stable microvessels in ischemia

We next tested whether TRAIL-R activation could promote microvascular networks in *Trail*^{-/-} and *Trail*^{+/+} ECs. EC proliferation and tubule formation were increased with an agonistic anti-mouse TRAIL-R mAb, MD5-1 (Fig. 6, A and B). MD5-1 also increased angiogenic sprouting ex vivo, whereas *Trail-R*^{-/-} aortic rings exhibited impaired sprouting (Fig. 6, C and D). In HMEC-1, agonistic TRAIL-R2 mAb stimulated proliferation, migration, and tubule formation (Fig. 6, E to G). In contrast, TRAIL-R1 neutralization had no effect on TRAIL-dependent in vitro processes of angiogenesis (Fig. 6, H and I). We next administered MD5-1 directly to ischemic *Trail*^{EC-/-} limbs. MD5-1 restored blood perfusion and increased stable microvessel numbers at 7 days (Fig. 7, A and B), a finding associated with increased expression of *Hbegf*, *Erb2*, and *Egfr* mRNA (Fig. 7C). In contrast, *Trail-R*^{-/-} ischemic limbs had reduced blood perfusion and reduced stable microvessel numbers after HLI (Fig. 7, D and E); no change in large vessel numbers was observed with treatment or genotype (fig. S5, B and C). Furthermore, Conatumumab increased sprouting by >50% in blood vessels isolated from ischemic regions of human amputated limbs (Fig. 7, F and G). Collectively, these indicate that TRAIL receptor activation stimulates stable microvessel formation and repurposing Conatumumab, an agonistic TRAIL-R2 mAb developed for

cancer therapy, could be a very real possibility in stimulating stable blood vessel networks as a treatment of PAD.

DISCUSSION

Patients with PAD have a higher risk of all-cause cardiovascular mortality, with a risk of stroke or heart attack equal to patients with coronary artery disease (24). Even after successful revascularization, the systemic health impact of PAD persists, with more hospitalizations, reinterventions, and reduced life expectancy versus any other patient group with atherosclerosis (25). With no major advances in revascularization techniques in the last two decades, an approach to increase blood perfusion by injection of therapeutics to improve vessel function and stimulate stable microvascular networks could be life-changing for these patients. This study sought to identify the critical molecules involved in reversing the effects of ischemia. We discovered five key findings: (i) the endothelium is a major source of TRAIL in the circulation; (ii and iii) EC-derived TRAIL stimulated stable microvascular networks forming EC tubes, recruiting pericytes, increasing pericyte wrapping, and prolonging microvessel survival. Notably, the importance of the HBEGF pathway in TRAIL-dependent EC-pericyte communications was identified. (iv) TRAIL was suppressed in PAD, associating with impaired EC function, and reduced stable microvessel numbers with ischemia; and (v) activating the TRAIL-R2 in vitro, in preclinical PAD, and ex vivo in human blood vessels isolated from patient amputations increased stable microvessel networks. A summary of these findings is illustrated in Fig. 8. Our study provides knowledge as to how EC-derived TRAIL promotes microvessel development in ischemia, characterizing non-apoptotic functions and

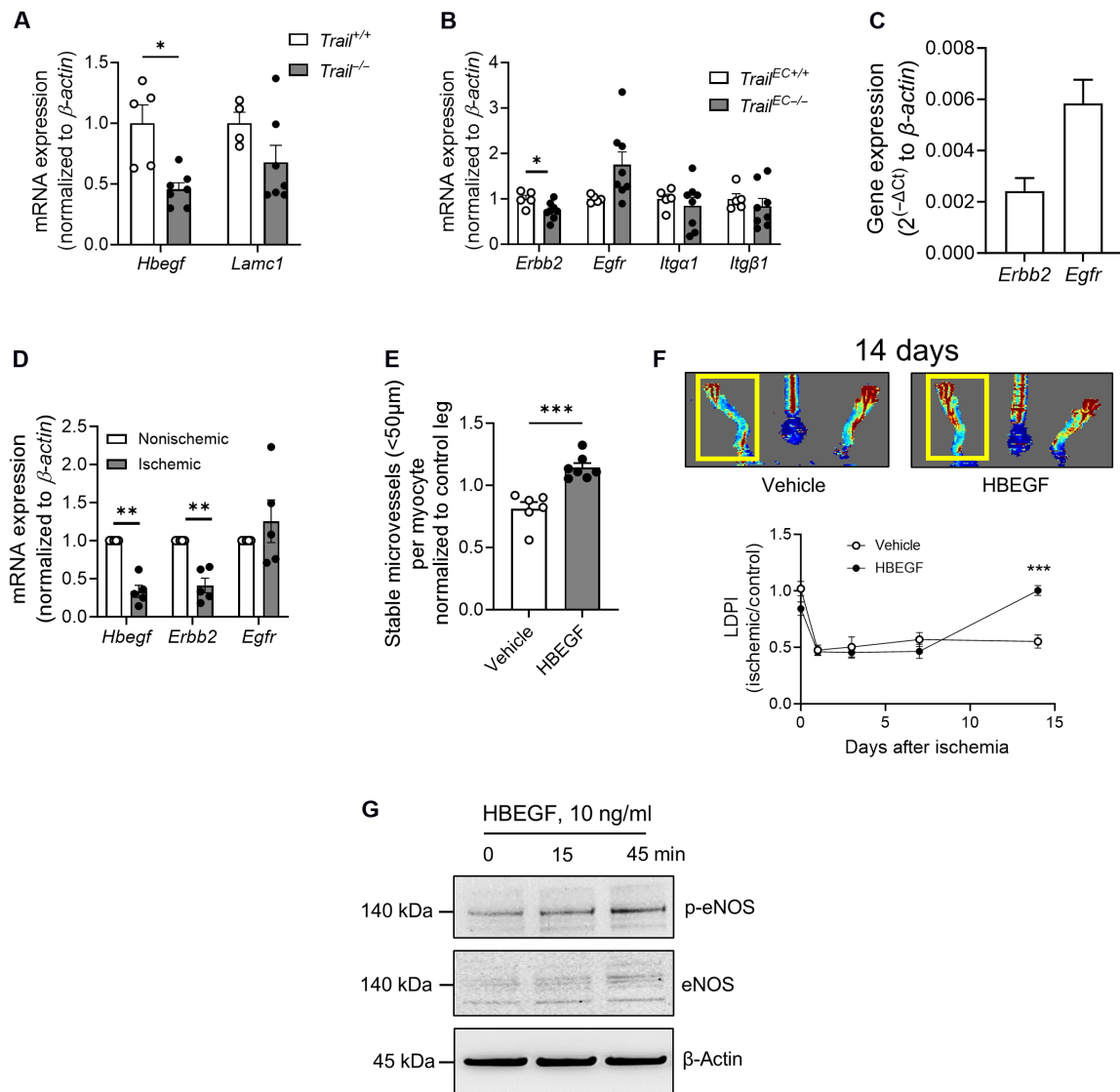


Fig. 5. EC-pericyte interactions are altered in ischemic limbs of *Trail*^{EC-/-} mice. (A) *Hbegf* and *Lamc1* mRNA levels in ECs isolated from *Trail*^{+/+} and *Trail*^{-/-} mice ($n = 4$ to 7 per genotype). (B) mRNA expression of *Hbegf* receptors *Erbb2* and *Egfr*, and *Lamc1* receptors *Itga1* and *Itgb1* in gastrocnemius muscle from *Trail*^{EC+/+} and *Trail*^{EC-/-} mice ($n = 5$ to 8 per genotype). (C) *Erbb2* and *Egfr* expression in primary murine pericytes. (D) mRNA expression of *Hbegf* receptors *Erbb2* and *Egfr* in nonischemic and ischemic skeletal muscle from patients with PAD ($n = 5$). (E) Stable microvessel numbers in gastrocnemius muscle of *Trail*^{EC-/-} mice treated with vehicle or recombinant murine HBEGF and 14 days after HLI ($n = 6$ to 7 per treatment). (F) Laser Doppler imaging showing blood perfusion over time in *Trail*^{EC-/-} mice treated with vehicle or recombinant HBEGF (1 μ g I.M., 2 days before surgery, day of surgery, and then daily). Top: Representative image of blood flow at 14 days. Bottom: Quantification ($n = 6$ to 7 per treatment). (G) Recombinant human HBEGF increases eNOS expression and phosphorylation (p-eNOS) in HMEC-1. β -Actin demonstrates unbiased loading. All mRNA expression was normalized to β -actin. Student's *t* test, paired *t* test, or two-way ANOVA; * $P < 0.05$ and *** $P < 0.001$.

laying the foundations for TRAIL receptor agonists for therapeutic use in people with ischemic vascular conditions.

ECs play an essential role in vascular homeostasis, and EC dysfunction contributes to every stage of PAD (26). Our work previously revealed the non-apoptotic effects of TRAIL in ECs. Specifically, physiological doses of TRAIL protected ECs from death, reduced EC reactivity, and improved endothelial integrity in response to oxidative damage (13). Global TRAIL deletion in mice also impaired endothelial-dependent arterial vasodilation, increased inflammation, and accelerated atherosclerosis (6, 7, 10, 11, 13), whereas TRAIL

promoted angiogenesis by increasing p-eNOS and nitric oxide production (15, 27) in a NOX4-mediated manner (11), a finding supported by others (17, 28). It is important to note the limitations of the HLI model of PAD. While this model induces lower extremity ischemia, it is more representative of acute limb ischemia, rather than a chronic atherosclerosis model. Nevertheless, our findings are important because TRAIL levels are reduced in patients with atherosclerotic diseases (7, 13, 29) and circulating TRAIL levels predict poor prognosis in coronary artery disease (30, 31), heart failure (31), and acute myocardial infarction (32), but its role in

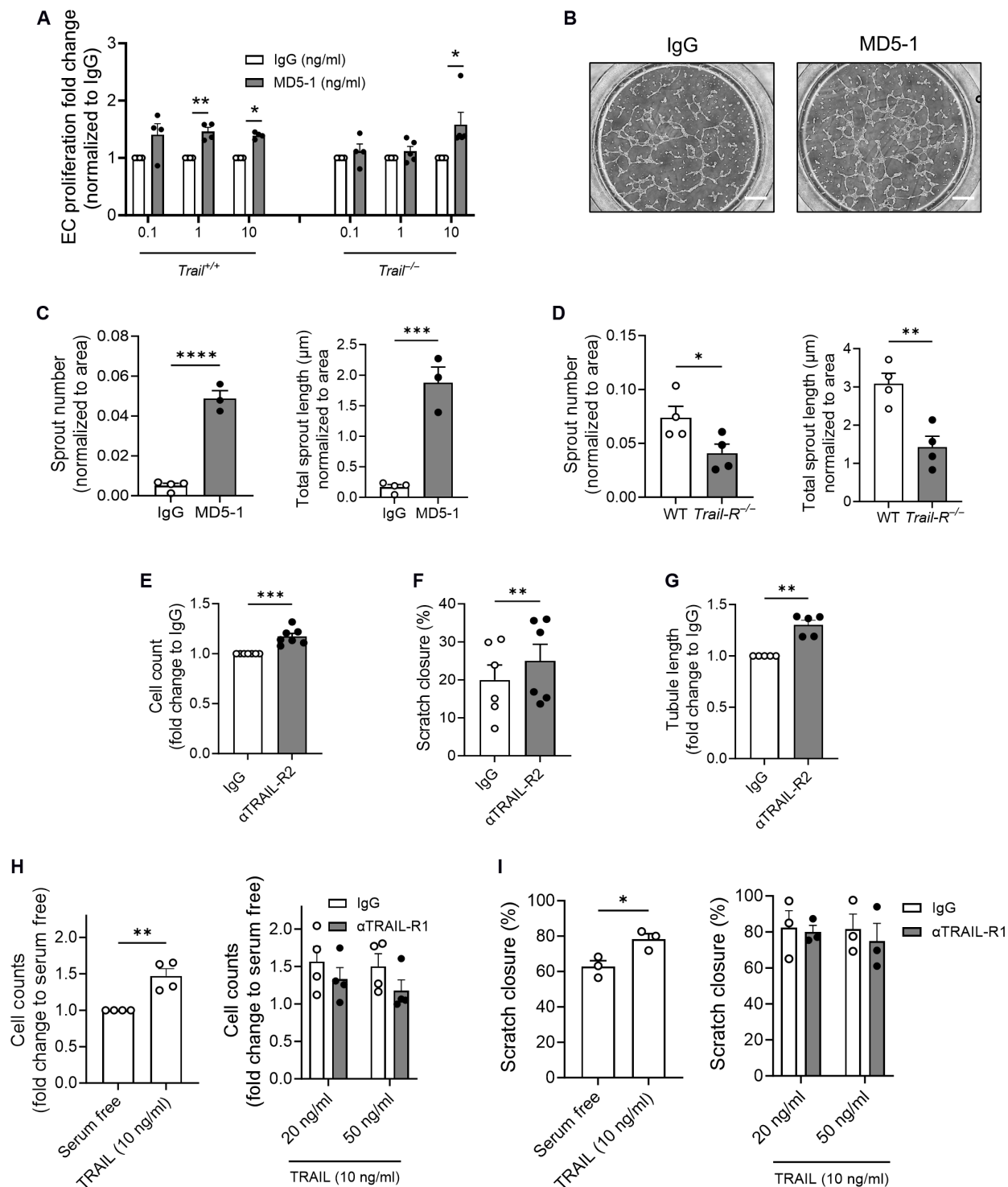


Fig. 6. TRAIL-receptor activation stimulates features of neo-angiogenesis. (A) *Trail*^{+/+} and *Trail*^{-/-} EC proliferation is increased with MD5-1 at 24 hours, normalized to immunoglobulin G (IgG; $n = 4$ to 5 per group). (B) Representative images showing increased tubule formation of *Trail*^{+/+} ECs with MD5-1 versus IgG at 6 hours (10 ng/ml); scale bars, 500 μm. (C) Aortic rings from wild-type mice were exposed to MD5-1 or IgG for 4 days, and sprout number and total sprout length were assessed ($n = 3$ to 4 per group). (D) Aortic rings from *Trail-R*^{-/-} mice exposed to hypoxia for 6 days have reduced sprout number and reduced total sprout length ($n = 4$ per group). Human TRAIL-R2 agonistic antibody (αTRAIL-R2, 10 ng/ml) stimulates HMEC-1 (E) proliferation, (F) migration, and (G) tubule formation ($n = 5$ to 7 per group). Conversely, neutralization by αTRAIL-R1 has no effect on TRAIL-inducible HMEC-1 (H) proliferation and (I) migration ($n = 3$ to 4 per group). Results are means ± SEM; two-way ANOVA, Mann-Whitney *U* test, or Student's *t* test; * $P < 0.05$, ** $P < 0.01$, *** $P < 0.001$, and **** $P < 0.0001$.

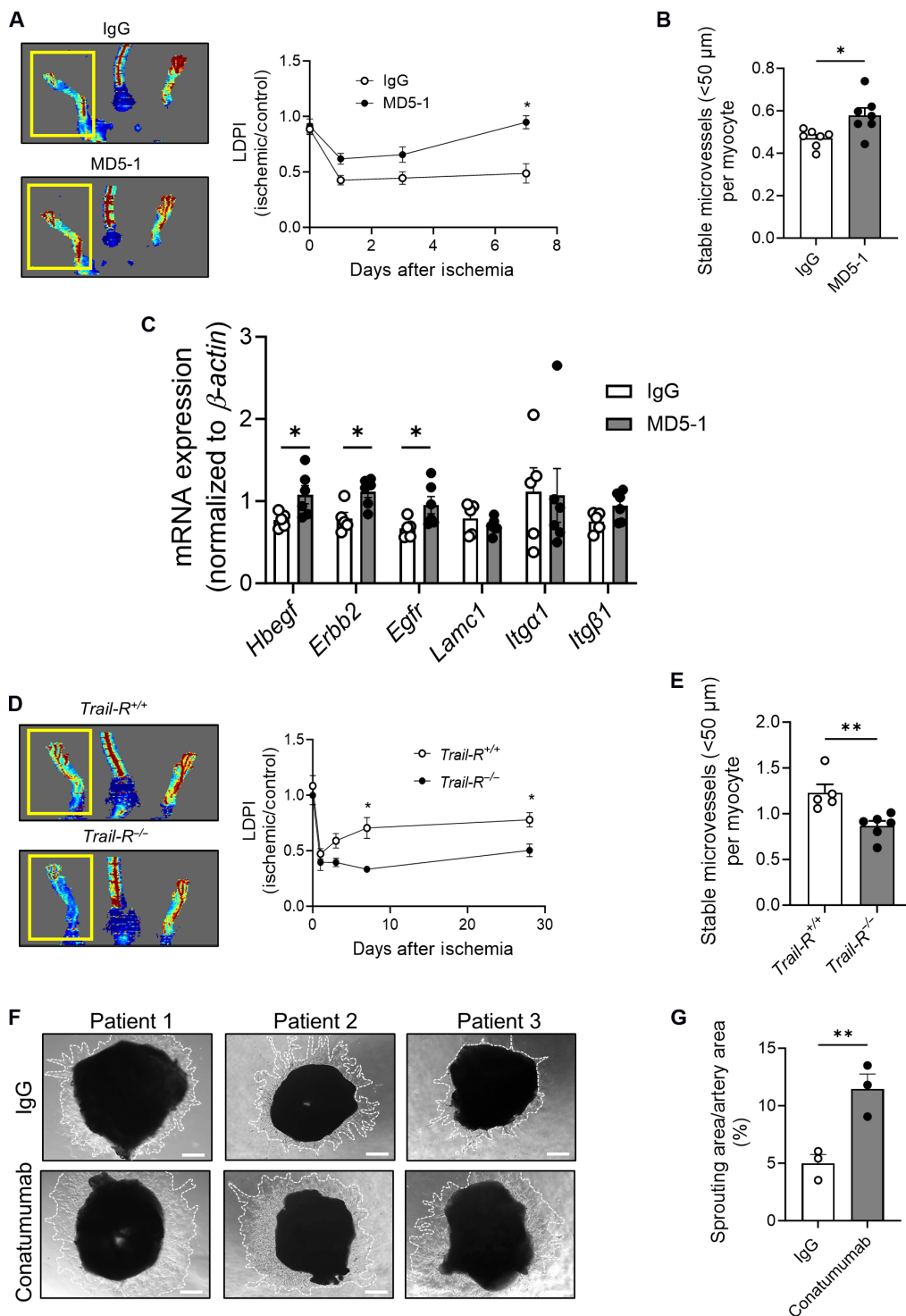


Fig. 7. TRAIL-R2 activation stimulates angiogenesis. (A) Laser Doppler imaging showing blood perfusion in HLI *Trail^{EC-/-}* mice treated with MD5-1 or IgG over 7 days (1 μg I.M., 2 days before, 2 days after, and 6 days after surgery). Left: Representative image at 7 days. Right: Quantification over time and (B) stable microvessel numbers (CD31⁺SMA⁺) in gastrocnemius from ischemic limbs ($n = 6$ to 7 per group). (C) mRNA expression of *Hbegf* and its receptors *ErbB2* and *Egfr*, and *Lamc1* and its receptors *Itga1* and *Itgb1* in gastrocnemius muscle of mice, normalized to β -actin ($n = 5$ to 6 per genotype). (D) Laser Doppler imaging showing blood perfusion in HLI *Trail-R^{+/+}* and *Trail-R^{-/-}* mice over 28 days. Left: Representative image at 28 days. Right: Quantification over time and (E) stable microvessel numbers (CD31⁺SMA⁺) in gastrocnemius from ischemic limbs 28 days after HLI ($n = 5$ to 6 per group). (F) Sprouting in blood vessels harvested from ischemic tissues of patients with PAD undergoing below-knee amputation. Vessels were exposed to Conatumumab or IgG (500 ng/ml) for 7 days; scale bars, 200 μm . (G) Quantification of sprout area (white dotted lines), normalized to vessel segment area using ImageJ ($n = 3$ per treatment). Results are means \pm SEM; Student's *t* test; * $P < 0.05$ and ** $P < 0.01$.

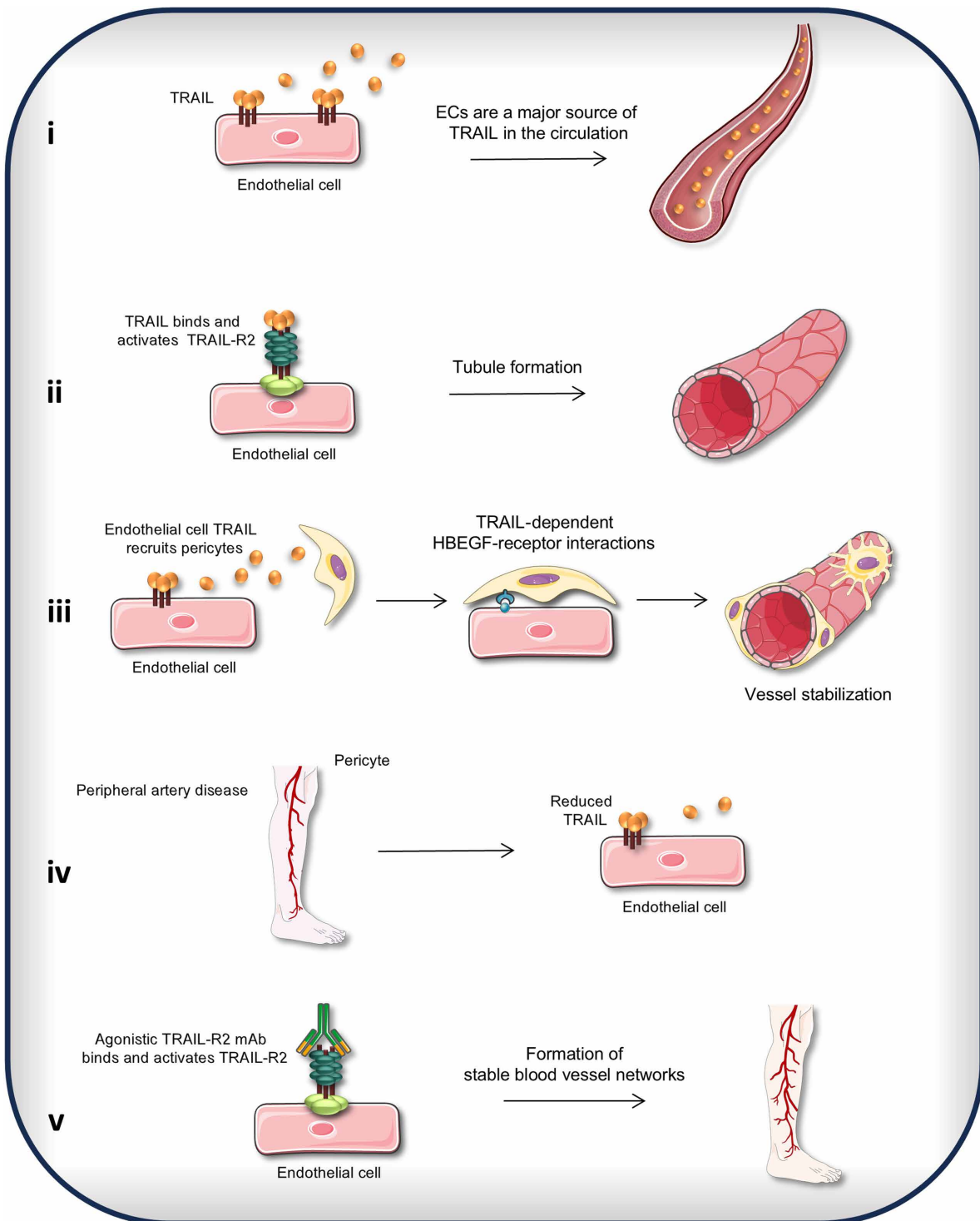


Fig. 8. TRAIL-dependent EC-pericyte interactions generate stable microvessel formation. (i) ECs are a major source of TRAIL in the circulation. (ii) TRAIL binds and activates TRAIL-R2 to stimulate the formation of immature microvessels. (iii) EC-derived TRAIL recruits pericytes to the endothelium to form stable blood vessel networks. EC-pericyte communication is mediated by HBEGF and HBEGF receptor interactions. (iv) EC-derived TRAIL is suppressed in PAD. (v) Agonistic TRAIL-R2 mAb stimulates the formation of stable microvessels in PAD.

PAD is unclear. We previously estimated that ~30% of plasma TRAIL was derived from cells originating in the bone marrow (7). We now show that ~60% of TRAIL in the circulation is produced by the endothelium but suppressed in patients with high-risk PAD. scRNA-seq data from muscle biopsies showed reduced *Trail* mRNA in ECs (33) and in capillaries (34) from PAD versus healthy age-matched individuals, supporting our work. Our findings suggest that reduced TRAIL levels in the circulation and tissue reflect impaired EC function(s). How the newly identified downstream gene targets affect TRAIL-dependent EC processes in PAD pathophysiology is now unknown and requires further elucidation.

Pericytes reside within the basement membrane of microvessels including in terminal arterioles, precapillary venules, and capillaries, adhering to the surface of ECs via peg-socket interactions. The resulting connection and cross-talk influence the formation, stabilization, and remodeling of the microvasculature. We discovered that EC-derived TRAIL is a molecular facilitator of EC-pericyte cross-talk mediated by HBEGF. *Hbegf* mRNA was reduced in ECs lacking TRAIL but increased in *Trail*^{EC-/-} limbs treated with MD5-1. HBEGF administration improved blood perfusion in *Trail*^{EC-/-} ischemic limbs by increasing the formation of stable microvessels. Given that agonistic TRAIL-R2 stimulates the EGFR in cardiomyocytes (35), TRAIL signaling may be a common upstream mechanism activating this pathway. Patients with PAD have reduced plasma HBEGF levels (36), further supporting our findings. While the current study focused on HBEGF, other EC-pericyte pathways were also identified and absent with TRAIL deletion in the endothelium including PDGFβ-PDGFRα. EC-pericyte communication is complex and intricately linked. HBEGF and PDGFβ jointly regulate pericyte recruitment and vessel stabilization (20), but whether TRAIL-HBEGF-PDGFRβ signals collectively mediate EC-pericyte processes for effective microvessel formation and stabilization is not clear.

In this study, we show that TRAIL-R activation stimulates stable microvessel formation in ischemia. In contrast, studies in cancer showed that activation of TRAIL-R on tumor ECs promoted apoptosis, disrupted endothelial integrity, and attenuated tumor growth in mice (37). EC-specific TRAIL deletion in mice did not affect tumor growth or tumor vascularization, instead lung metastasis was increased (38), with greater intracellular versus cell surface TRAIL expression (38). This highlights the complexity of TRAIL signaling under altered conditions. To stimulate apoptosis, cancer treatments often use much greater levels of TRAIL and MD5-1 (37, 39) compared to the concentrations used in the current study. Super clustering of signaling receptors allows for higher order oligomerization, which promotes apoptosis via lipid rafts, whereas non-raft-mediated TRAIL receptor interactions stimulate survival pathways (40, 41). In addition to binding TRAIL-R1 and TRAIL-R2 in humans, TRAIL can also bind three decoy receptors (DcR1, DcR2, and osteoprotegerin). In mice, only osteoprotegerin has been identified as a decoy receptor at the protein level. How TRAIL interacts with its decoy receptors or the functional consequence of this in our study is unknown. Whether differences in phenotype between cardiovascular disease and cancer are attributed to intracellular or extracellular TRAIL detection and/or receptor expression is uncertain.

In contrast to TRAIL's apoptosis-inducing effects in cancer, we have shown that activation of TRAIL signals improves vascular homeostasis in PAD, potentially reducing the incidence of amputation. MD5-1 treatment stimulated stable microvessels in ischemia, improving blood perfusion to the lower limbs in mice, and Conatumumab

increased angiogenic sprouts from patient arteries ex vivo. Our study highlights the genuine potential for future trials to fast track Conatumumab or other TRAIL-R2 agonists already available for human use with more timely treatment of PAD.

MATERIALS AND METHODS

Human studies

Patients ≥ 18 years old presenting with chronic limb-threatening ischemia, requiring below knee amputation at Royal Prince Alfred Hospital, Sydney, Australia, were recruited. Healthy individuals ≥ 18 years old were also recruited for blood sampling. Exclusion criteria for the healthy cohort included known peripheral vascular disease, cardiovascular disease, cerebrovascular disease, and autoimmune disease. Patients and healthy individuals gave a written informed consent. Blood plasma was isolated, snap frozen, and stored at -80°C. After the limb was surgically removed, skeletal muscle from the tibialis anterior (close to the amputation site; nonischemic) and flexus hallucis longus (ischemic) were collected, fixed in formalin, or snap frozen. For myography, arteries were dissected from subcutaneous fat within the nonischemic or ischemic regions (lateral midfoot). All procedures were approved by the Sydney Local Health District Human Ethics Committee (X20-0183; Sydney, Australia).

Animal studies

Trail^{-/-} mice were originally sourced from Amgen (42). *Trail-R*^{-/-} mice were provided by G. Gores (Mayo Clinic, Minnesota, USA). Mice were rederived (C57BL/6J background) and bred at Australian BioResources. C57BL/6J mice were also purchased from Australian BioResources. A mix of male and female adult mice was used. Mice were housed with 12:12-hour light-dark cycles with free access to food and water. Mice were anesthetized by inhalation of 3% isoflurane prior to euthanasia via cardiac exsanguination or cervical dislocation. Blood plasma was stored at -80°C. Indicated tissues were harvested, either snap frozen or formalin fixed. All procedures were approved by the Sydney Local Health District Animal Welfare Committee (2014-027, 2017-020, 2017-024, 2019-030, and 2021-015; Sydney, Australia) and Sydney Local Health District Institutional Biosafety Committee (13-019, 18-021, and 23-027; Sydney, Australia).

Sex as a biological variable

Although samples included both sexes, sex was not considered as a biological variable in this study.

Generation of *Trail*^{EC-/-} mice

Mice with *Trail* floxed allele were generated by Ozgene (Bentley, Australia). To create a targeted vector, a flippase recognition target (FRT)-flanked phosphoglycerate kinase 1 neomycin cassette was inserted downstream of exon 5 of the *Trail* gene, flanked by LoxP sites. The construct was electroporated into genomic DNA of embryonic stem (ES) cells from C57BL/6J mice. The targeted ES cells were injected into C57BL/6J blastocysts to produce chimeric mice, which were crossed with C57BL/6J mice to generate *Trail*^{+^{flox-neo}-/-} mice. The FRT-flanked neomycin cassette was removed by crossing with *Rosa26-FlpE* mice. These mice were crossed with *VE-Cadherin Cre* (Jackson Laboratory) to generate EC-specific *Trail*^{-/-} (*Trail*^{EC-/-}) mice. Genotyping primer sequences are wild-type primer_01 forward: ATGGACCTGGATCAAGAAGCC and primer_02 reverse: GTCTCTCGATGAAACACCGAAAG producing a product of 252 base

pairs (bp); and TRAIL knockout primer_04 forward: CTTTGAC-CCCACCACAGTCTAATC and primer_02 reverse producing a product of 511 bp. For Cre, we used the following primers: 2173_transgene forward CCAGGCTGACCAAGCTGAG and 2174_transgene reverse CCTGGCGATCCCTGAACA.

Hindlimb ischemia

Hindlimb ischemia surgeries were performed as previously described (11). Briefly, mice were anesthetized with isoflurane, then the proximal and distal ends of the left femoral artery were ligated, and the artery and side branches were dissected free. The right leg was used as a control. Where described, 1 μ g of recombinant mouse HBEGF or vehicle control (saline) was administered by intramuscular (I.M.) injection in the ischemic gastrocnemius 2 days before surgery, on the day of surgery, and then daily for 14 days (endpoint). MD5-1 or immunoglobulin G (IgG; 1 μ g; control) was administered by I.M. injection in the ischemic gastrocnemius 2 days before, 2 days after, and 6 days after surgery, with endpoint at 7 days.

Myography

Isolated subcutaneous fat was placed in a modified Krebs-Henseleit solution. Arteries (277 ± 10 μ m, SEM diameter; $n = 4$ segments per patient) were dissected, cleaned, and cut into 2-mm segments that were mounted on tungsten wires (40 μ m diameter) on a myograph (Danish Myo Technology) at 37°C in Krebs-Henseleit solution and gassed with 5% CO₂ in O₂. Tension was measured using isometric force displacement transducers and recorded using LabChart V8Pro (ADInstruments). Once mounted, arteries were normalized to an internal diameter that produced 90% of 13.3 kPa (43). Arteries were contracted using 120 mM KCl until a stable contraction was reached, then washed out, rested for 30 min, and tested for endothelium-dependent relaxation using acetylcholine or endothelium-independent relaxation using sodium nitroprusside.

Tissue culture

HMEC-1 (Centers for Disease Control and Prevention, MTA M1224I) were maintained in MCDB 131 medium (Gibco) including supplements (11). The pericyte precursor cell line, 10 T1/2 (American Type Culture Collection), was cultured in Dulbecco's modified Eagle's medium (DMEM; Gibco) (44). Primary ECs were isolated and cultured as described (45). Primary pericytes were isolated and cultured in 2% serum-containing pericyte medium (ScienCell) (46). Cells were maintained at 37°C in a humidified atmosphere of 5% CO₂. In hypoxia (2% O₂), cells were maintained in serum-deprived conditions. Primary ECs were not used beyond passages 1 and 2. Pericytes were not used after nine passages.

RNA isolation and qPCR

RNA was isolated from cells and tissues using TRI Reagent (Sigma-Aldrich) or the RNeasy Fibrous Tissue Mini Kit (QIAGEN) (7, 8, 11). cDNA was generated using the iScript cDNA synthesis kit (Bio-Rad, Australia), and qPCR was performed using iQ SYBR (Bio-Rad, Australia) in a CFX96 thermocycler (Bio-Rad, Australia). The $\Delta\Delta$ CT method was used to assess relative mRNA changes, normalized to β -actin or *Hprt*. Primer sequences are in table S6.

Western blotting

Western blotting was performed as previously described (13). Cellulose membranes were incubated with antibodies to TRAIL-R1

(1:200, overnight 4°C, R&D Systems), p-eNOS (1:500, overnight 4°C, Cell Signaling Technology), eNOS (1:500, overnight 4°C, Cell Signaling Technology), and β -actin (1:5000, 1 hour at room temperature; Sigma-Aldrich). Proteins were detected with horseradish peroxidase-conjugated secondary anti-goat, anti-mouse, or anti-rabbit antibodies (1:1000, 1 hour at room temperature, Dako) and visualized using the ChemiDoc MP imaging system (Bio-Rad).

Total internal reflection fluorescence microscopy

HMEC-1 cultured on glass bottom 35-mm dish (FluoroDish) were formalin fixed and stained with anti-TRAIL antibody (1:100, overnight 4°C, Abcam) and anti-rabbit Alexa 647 (1 hour at room temperature, Thermo Fisher Scientific). Phalloidin-Alexa488 (1:500, 30 min at room temperature, Thermo Fisher Scientific) was used to detect actin. Images were captured using an Olympus cellTIRF-4Line system based on an Olympus IX81 inverted microscope (47).

Flow cytometry

HMEC-1 were blocked in 10% bovine serum albumin and then stained with anti-human TRAIL-R2 mAb (20 μ g/ml; Novus Biological) or IgG (Life Technologies) and anti-rabbit fluorescein isothiocyanate (FITC; 1:500, BD Biosciences) for 45 min at 4°C. Cells were fixed with 10% formalin and run on a BD FACSVerser Flow Cytometer. Data analyzed with FlowJo (v10.8.1), and geometric mean of viable populations was quantified.

Duolink proximity ligation assay

Duolink Proximity Ligation Assay (Sigma-Aldrich) was performed according to the manufacturer's instructions. Cells were incubated with primary mAb (1 μ g/ml; TRAIL-R2, Novus-Biologicals; TRAIL-R1, Abcam; and TRAIL, Abcam or R&D Systems) or appropriate IgG overnight at 4°C. Slides were mounted with 4',6-diamidino-2-phenylindole (DAPI) Fluoromount-G (SouthernBiotech) and imaged using the Zeiss Axio Imager Z2. Six images were captured per group and analyzed with ImageJ. The red fluorescence intensity per image was quantified and normalized to the number of DAPI-positive nuclei.

Human enzyme-linked immunosorbent assays

TRAIL (R&D Systems) and TRAIL-R2 (Abcam) were measured in plasma according to the manufacturer's instructions.

Histology

Immunofluorescence was performed on formalin-fixed 5- μ m sections with the following antibodies. Human: CD31 (R&D Systems), smooth muscle α -actin (SMA; Sigma-Aldrich), and laminin (Novus Biologicals); mouse: CD31 (Abcam or R&D Systems), smooth muscle actin (Sigma-Aldrich), and laminin (Novus Biologicals). Slides were mounted with DAPI Fluoromount-G mounting medium. Control sections were negative. Hematoxylin and eosin, Van Gieson's, and Picrosirius red stains were performed on aortae. Images were captured using a Zeiss Axio Imager Z2 or Zeiss Axio Scan.Z1 microscope and analyzed with Zen 3.6 software (Zeiss) or ImageJ.

Mouse plasma chemistries

Plasma glucose was measured by glucometer (Lifesmart). Insulin (Mercodia), cholesterol, (Wako Diagnostics), and TRAIL (Cloud-Clone Corp.) were assessed according to the manufacturer's instructions.

Permeability assay

Adult mice injected intravenously with 200 μ l of 0.5% Evans Blue (Sigma-Aldrich) were euthanized 30 min later. Tissue was collected and Evans Blue was extracted as described (13).

Matrigel plug assay

Matrigel (500 μ l; growth factor reduced; Corning) containing 500 ng of fibroblast growth factor-2 (Sigma-Aldrich) was injected subcutaneously into the flank of mice. Plugs were harvested at 28 days and fixed in formalin for immunofluorescence or snap frozen for gene expression.

Tubulogenesis assays

Serum-arrested primary murine ECs or HMEC-1 were seeded onto Matrigel coated μ -Slide Angiogenesis plates (iBidi) or 96-well plates in serum-free or 1% fetal bovine serum (FBS)-containing medium. Images were captured using a Zeiss 800 microscope at indicated times. Area of tubule formation was measured by WimTube on Wimasis Image Analysis, or the number of tubules per field of view was counted using ImageJ.

Cell proliferation

Cells were seeded into 96-well plates (10,000 cells per well) and, the following day, were serum arrested for 24 hours. Cells were treated with antibodies or recombinant human TRAIL (R&D Systems) as indicated. Total cell numbers per well were counted 24 hours later using a haemocytometer or Coulter Counter (Beckman). Where relevant, cell counts were normalized to their respective controls.

Migration assay

Transwell assay: 50,000 serum-arrested cells were seeded into 8- μ m-pore transwell inserts. After 8 hours of migration, the membranes were washed (phosphate-buffered saline), fixed, and stained with DiffQuik. Images were captured using an Olympus IX70 microscope. Migrated cells (as a measure of fold change compared to control) per field of view was determined. Scratch assay: Serum-arrested cells in six-well plates were scratched using a sterile P20 tip. Images of the scratch before and 24 hours following treatment were captured using an Olympus IX71. Scratch area before and after cell migration was measured using ImageJ to determine % of scratch closure (48).

Single-cell RNA sequencing

Gastrocnemius muscle was collected, prepared (49), and pooled ($n = 2$ per genotype) for mouse studies. Human tissues collected (Fig. 2C) from one patient were also prepared. The 10x Genomics Chromium System (10x Genomics Inc., San Francisco, CA) was used. scRNA-seq libraries were generated following capture (50). Raw scRNA-seq reads were processed (Cell Ranger, v6.0.2) (50) and aligned to the mouse (mm10-20202-A) or human (GRCh38-2020-A) reference transcriptome. Downstream analysis was performed in R (v4.2.3); quality control was conducted using Seurat (v4.3.0), SeuratObject (v4.1.3) (51), and DoubletFinder (v2.0.3) (52). Data clustering, visualization, and DEG analysis were performed using Seurat (v4.3.0). The quality control and clustering steps for mouse and human sequences are shown in tables S7 and S8. Expression matrices were normalized and scaled by Seurat's "SCTransform" method. Cell clusters were annotated using known cell markers (fig. S6B). EC/pericyte clusters were further analyzed. DEGs were determined using Seurat's "FindMarkers." Genes

were considered significantly differentially expressed when expressed in at least 10% of cells analyzed with adjusted P value of <0.05 . DEGs were displayed using EnhancedVolcano (v1.20.0). Enriched gene ontology (GO) terms were identified by overexpression analysis using clusterProfiler (53). GO terms with P value of <0.05 and q value of <0.1 were considered significantly enriched. Cell-cell interactions were investigated using CellChat (19). Differences in ligand-receptor pairs were determined using "netVisual_bubble" function comparison parameter and considered significant with a P value of <0.05 .

MD5-1

MD5-1 was purified from hybridomas (54). Effects of MD5-1 were compared to those of hamster IgG (LifeSpan Biosciences).

Aortic explant sprouting assay

Aortic rings (1 mm) were transferred to Matrigel-coated wells, overlaid with additional Matrigel, and incubated in DMEM (Sigma-Aldrich) with 10% FBS, L-glutamine, penicillin, and streptomycin. Vessels were placed in normoxic/hypoxic conditions, and antibodies were applied as indicated. Medium containing antibodies was replaced every 2 to 3 days. Images were captured at indicated times using an Olympus IX71 microscope. Sprout number was counted, and the total length of all sprouts was measured using ImageJ. A minimum of two to three vessel segments per treatment per genotype were analyzed and averaged.

Human vessel sprouting

Blood vessels from ischemic region of amputated limbs were collected, cut into 1- to 2-mm rings, then transferred to Matrigel-coated wells, and overlaid with additional Matrigel. Segments were incubated in MCDB 131 medium (Gibco) containing 5% FBS, hydrocortisone, epidermal growth factor, L-glutamine, and penicillin/streptomycin, with Conatumumab (500 ng/ml; obtained from Amgen, master agreement number 2013583585) or control IgG. Medium containing antibodies was replaced every 2 to 3 days. Images were captured using an Olympus IX71 microscope at day 7. Sprouting area was outlined, and sprout area was quantified and normalized to the vessel area using ImageJ. A minimum of two to three vessel segments per treatment per patient were analyzed and averaged.

Statistics

Results expressed as means \pm SEM. Statistical comparisons were made using Students t tests, Mann-Whitney U test, one- or two-way analysis of variance (ANOVA), with Bonferroni's or Šidák's multiple comparisons posttest, where appropriate. Outliers were identified and excluded. Unless indicated, GraphPad Prism version 10.01 was used. $P < 0.05$ was considered significant.

Supplementary Materials

The PDF file includes:

Figs. S1 to S8
Tables S1 to S8
Legend for data S1
References

Other Supplementary Material for this manuscript includes the following:

Data S1

REFERENCES AND NOTES

- P. Song, D. Rudan, Y. Zhu, F. J. I. Fowkes, K. Rahimi, F. G. R. Fowkes, I. Rudan, Global, regional, and national prevalence and risk factors for peripheral artery disease in 2015: An updated systematic review and analysis. *Lancet Glob. Health* **7**, e1020–e1030 (2019).
- K. Ziegler-Graham, E. J. MacKenzie, P. L. Ephraim, T. G. Travison, R. Brookmeyer, Estimating the prevalence of limb loss in the United States: 2005 to 2050. *Arch. Phys. Med. Rehabil.* **89**, 422–429 (2008).
- C. Emanuelli, P. Madeddu, Angiogenesis gene therapy to rescue ischaemic tissues: Achievements and future directions. *Br. J. Pharmacol.* **133**, 951–958 (2001).
- R. Cao, Y. Xue, E. M. Hedlund, Z. Zhong, K. Tritsaris, B. Tondelli, F. Lucchini, Z. Zhu, S. Dissing, Y. Cao, VEGFR1-mediated pericyte ablation links VEGF and PIGF to cancer-associated retinopathy. *Proc. Natl. Acad. Sci. U.S.A.* **107**, 856–861 (2010).
- N. S. Azahri, M. M. Kavaruma, Transcriptional regulation of tumour necrosis factor-related apoptosis-inducing ligand. *Cell. Mol. Life Sci.* **70**, 3617–3629 (2013).
- S. P. Cartland, J. H. Erlich, M. M. Kavaruma, TRAIL deficiency contributes to diabetic nephropathy in fat-fed ApoE^{-/-} mice. *PLOS ONE* **9**, e92952 (2014).
- S. P. Cartland, S. W. Genner, G. J. Martinez, S. Robertson, M. Kockx, R. C. Lin, J. F. O'Sullivan, Y. C. Koay, P. Manuneedhi Cholan, M. A. Kebede, A. J. Murphy, S. Masters, M. R. Bennett, W. Jessup, L. Kritharides, C. Ceczy, S. Patel, M. M. Kavaruma, TRAIL-expressing monocyte/macrophages are critical for reducing inflammation and atherosclerosis. *iScience* **12**, 41–52 (2019).
- S. P. Cartland, H. H. Harith, S. W. Genner, L. Dang, V. C. Cogger, M. Vellozzi, B. A. Di Bartolo, S. R. Thomas, L. A. Adams, M. M. Kavaruma, Non-alcoholic fatty liver disease, vascular inflammation and insulin resistance are exacerbated by TRAIL deletion in mice. *Sci. Rep.* **7**, 1898 (2017).
- J. Chan, L. Prado-Lourenco, L. M. Khachigian, M. R. Bennett, B. A. Di Bartolo, M. M. Kavaruma, TRAIL promotes VSMC proliferation and neointima formation in a FGF-2-, Sp1 phosphorylation-, and NFκB-dependent manner. *Circ. Res.* **106**, 1061–1071 (2010).
- B. Di Bartolo, J. Chan, M. Bennett, S. Cartland, S. Bao, B. Tuch, M. Kavaruma, TNF-related apoptosis-inducing ligand (TRAIL) protects against diabetes and atherosclerosis in ApoE^{-/-} mice. *Diabetologia* **54**, 3157–3167 (2011).
- B. A. Di Bartolo, S. P. Cartland, L. Prado-Lourenco, T. S. Griffith, C. Gentile, J. Ravindran, N. S. Azahri, T. Thai, A. W. Yeung, S. R. Thomas, M. M. Kavaruma, Tumor necrosis factor-related apoptosis-inducing ligand (TRAIL) promotes angiogenesis and ischemia-induced neovascularization via NADPH oxidase 4 (NOX4) and nitric oxide-dependent mechanisms. *J. Am. Heart Assoc.* **4**, e002527 (2015).
- M. M. Kavaruma, M. Schoppet, Y. V. Bobryshev, L. M. Khachigian, M. R. Bennett, Trail stimulates proliferation of vascular smooth muscle cells via activation of NF-κB and induction of insulin-like growth factor-1 receptor. *J. Biol. Chem.* **283**, 7754–7762 (2008).
- P. Manuneedhi Cholan, S. P. Cartland, L. Dang, B. S. Rayner, S. Patel, S. R. Thomas, M. M. Kavaruma, TRAIL protects against endothelial dysfunction in vivo and inhibits angiotensin-II-induced oxidative stress in vascular endothelial cells in vitro. *Free Radic. Biol. Med.* **126**, 341–349 (2018).
- S. P. Cartland, S. W. Genner, A. Zahoor, M. M. Kavaruma, Comparative evaluation of TRAIL, FGF-2 and VEGF-A-induced angiogenesis in vitro and in vivo. *Int. J. Mol. Sci.* **17**, 2025 (2016).
- P. Secchiero, A. Gonelli, E. Carnevale, F. Corallini, C. Rizzardi, S. Zacchigna, M. Melato, G. Zauli, Evidence for a proangiogenic activity of TNF-related apoptosis-inducing ligand. *Neoplasia* **6**, 364–373 (2004).
- H. M. Rosevear, A. J. Lightfoot, T. S. Griffith, Conatumumab, a fully human mAb against death receptor 5 for the treatment of cancer. *Curr. Opin. Investig. Drugs* **11**, 688–698 (2010).
- S. M. Craige, K. Chen, Y. Pei, C. Li, X. Huang, C. Chen, R. Shibata, K. Sato, K. Walsh, J. F. Keane Jr., NADPH oxidase 4 promotes endothelial angiogenesis through endothelial nitric oxide synthase activation. *Circulation* **124**, 731–740 (2011).
- E. Vazquez-Liebanas, K. Nahar, G. Bertuzzi, A. Keller, C. Betsholtz, M. A. Mae, Adult-induced genetic ablation distinguishes PDGFB roles in blood-brain barrier maintenance and development. *J. Cereb. Blood Flow Metab.* **42**, 264–279 (2022).
- S. Jin, C. F. Guerrero-Juarez, L. Zhang, I. Chang, R. Ramos, C. H. Kuan, P. Myung, M. V. Pliusk, Q. Nie, Inference and analysis of cell-cell communication using CellChat. *Nat. Commun.* **12**, 1088 (2021).
- A. N. Stratman, A. E. Schwindt, K. M. Malotte, G. E. Davis, Endothelial-derived PDGF-BB and HB-EGF coordinately regulate pericyte recruitment during vasculogenic tube assembly and stabilization. *Blood* **116**, 4720–4730 (2010).
- S. S. Kemp, K. N. Aguera, B. Cha, G. E. Davis, Defining endothelial cell-derived factors that promote pericyte recruitment and capillary network assembly. *Arterioscler. Thromb. Vasc. Biol.* **40**, 2632–2648 (2020).
- E. Iivanainen, L. Nelimarkka, V. Elenius, S. M. Heikkinen, T. T. Junttila, L. Sihombing, M. Sundvall, J. A. Maatta, V. J. Laine, S. Yla-Herttuala, S. Higashiyama, K. Alitalo, K. Elenius, Angiotensin-regulated recruitment of vascular smooth muscle cells by endothelial-derived heparin binding EGF-like growth factor. *FASEB J.* **17**, 1609–1621 (2003).
- M. Yoshizumi, S. Kourembanas, D. H. Temizer, R. P. Cambria, T. Quertermous, M. E. Lee, Tumor necrosis factor increases transcription of the heparin-binding epidermal growth factor-like growth factor gene in vascular endothelial cells. *J. Biol. Chem.* **267**, 9467–9469 (1992).
- G. Agnelli, J. J. F. Belch, I. Baumgartner, P. Giovias, U. Hoffmann, Morbidity and mortality associated with atherosclerotic peripheral artery disease: A systematic review. *Atherosclerosis* **293**, 94–100 (2020).
- S. J. Aitken, Peripheral artery disease in the lower limbs: The importance of secondary risk prevention for improved long-term prognosis. *Aust. J. Gen. Pract.* **49**, 239–244 (2020).
- M. M. Kavaruma, C. Bursill, C. P. Stanley, F. Passam, S. P. Cartland, S. Patel, J. Loa, G. A. Figtree, J. Golledge, S. Aitken, D. A. Robinson, Endothelial cell dysfunction: Implications for the pathogenesis of peripheral artery disease. *Front. Cardiovasc. Med.* **9**, 1054576 (2022).
- P. Secchiero, A. Gonelli, E. Carnevale, D. Milani, A. Pandolfi, D. Zella, G. Zauli, TRAIL promotes the survival and proliferation of primary human vascular endothelial cells by activating the Akt and ERK pathways. *Circulation* **107**, 2250–2256 (2003).
- J. Yu, E. D. deMuinck, Z. Zhuang, M. Drinane, K. Kauser, G. M. Rubany, H. S. Qian, T. Murata, B. Escalante, W. C. Sessa, Endothelial nitric oxide synthase is critical for ischemic remodeling, mural cell recruitment, and blood flow reserve. *Proc. Natl. Acad. Sci. U.S.A.* **102**, 10999–11004 (2005).
- S. P. Cartland, R. C. Y. Lin, S. Genner, M. S. Patil, G. J. Martinez, J. Y. Barraclough, B. Gloss, A. Misra, S. Patel, M. M. Kavaruma, Vascular transcriptome landscape of Trail^{-/-} mice: Implications and therapeutic strategies for diabetic vascular disease. *FASEB J.* **34**, 9547–9562 (2020).
- S. Volpato, L. Ferrucci, P. Secchiero, F. Corallini, G. Zuliani, R. Fellini, J. M. Guralnik, S. Bandinelli, G. Zauli, Association of tumor necrosis factor-related apoptosis-inducing ligand with total and cardiovascular mortality in older adults. *Atherosclerosis* **215**, 452–458 (2011).
- A. Niessner, P. J. Hohensinner, K. Rychli, S. Neuhold, G. Zorn, B. Richter, M. Hulsmann, R. Berger, D. Mortl, K. Huber, J. Wojta, R. Pacher, Prognostic value of apoptosis markers in advanced heart failure patients. *Eur. Heart J.* **30**, 789–796 (2009).
- P. Secchiero, F. Corallini, C. Ceconi, G. Parrinello, S. Volpato, R. Ferrari, G. Zauli, Potential prognostic significance of decreased serum levels of TRAIL after acute myocardial infarction. *PLOS ONE* **4**, e4442 (2009).
- C. G. Pass, V. Palzkill, J. Tan, K. Kim, T. Thome, Q. Yang, B. Fazzone, S. T. Robinson, K. A. O'Malley, F. Yue, S. T. Scali, S. A. Berceci, T. E. Ryan, Single-nuclei RNA-sequencing of the gastrocnemius muscle in peripheral artery disease. *Circ. Res.* **133**, 791–809 (2023).
- G. Turiel, T. Desgeorges, E. Masschelein, M. Birrer, J. Zhang, S. Engelberger, K. De Bock, Single cell compendium of the muscle microenvironment in peripheral artery disease reveals capillary endothelial heterogeneity and activation of resident macrophages. *BioRxiv* 545899 [Preprint]. 22 June 2023. <https://doi.org/10.1101/2023.06.21.545899>.
- L. A. Grisanti, TRAIL and its receptors in cardiac diseases. *Front. Physiol.* **14**, 1256852 (2023).
- B. Li, N. Djanapour, A. Zamzam, M. H. Syed, S. Jain, R. Abdin, M. Qadura, Angiogenesis-related proteins as biomarkers for peripheral artery disease. *Heliyon* **9**, e20166 (2023).
- N. S. Wilson, A. Yang, B. Yang, S. Couto, H. Stern, A. Gogineni, R. Pitti, S. Marsters, R. M. Weimer, M. Singh, A. Ashkenazi, Proapoptotic activation of death receptor 5 on tumor endothelial cells disrupts the vasculature and reduces tumor growth. *Cancer Cell* **22**, 80–90 (2012).
- C. Riera-Domingo, E. Leite-Gomes, I. Charatsidou, P. Zhao, G. Carra, F. Cappellesso, L. Mourao, M. De Schepper, D. Liu, J. Serneels, M. G. Alameh, V. V. Shuvaev, T. Geukens, E. Isnaldi, H. Prenen, D. Weissman, V. R. Muzykantov, S. Soenen, C. Desmedt, C. Scheele, A. Sablina, M. Di Matteo, R. Martin-Perez, M. Mazzone, Breast tumors interfere with endothelial TRAIL at the premetastatic niche to promote cancer cell seeding. *Sci. Adv.* **9**, eadd5028 (2023).
- J. D. Graves, J. J. Kordich, T. H. Huang, J. Piasecki, T. L. Bush, T. Sullivan, I. N. Foltz, W. Chang, H. Douangpanya, T. Dang, J. W. O'Neill, R. Mallari, X. Zhao, D. G. Branstetter, J. M. Rossi, A. M. Long, X. Huang, P. M. Holland, Apo2L/TRAIL and the death receptor 5 agonist antibody AMG 655 cooperate to promote receptor clustering and antitumor activity. *Cancer Cell* **26**, 177–189 (2014).
- K. Kucka, H. Wajant, Receptor Oligomerization and its relevance for signaling by receptors of the tumor necrosis factor receptor superfamily. *Front. Cell Dev. Biol.* **8**, 615141 (2020).
- M. M. Kavaruma, N. Y. Tan, M. R. Bennett, Death receptors and their ligands in atherosclerosis. *Arterioscler. Thromb. Vasc. Biol.* **28**, 1694–1702 (2008).
- L. M. Sedger, M. B. Glaccum, J. C. Schuh, S. T. Kanaly, E. Williamson, N. Kayagaki, T. Yun, P. Smolak, T. Le, R. Goodwin, B. Gliniak, Characterization of the in vivo function of TNF-alpha-related apoptosis-inducing ligand, TRAIL/Apo2L, using TRAIL/Apo2L gene-deficient mice. *Eur. J. Immunol.* **32**, 2246–2254 (2002).

43. D. Cheng, J. Talib, C. P. Stanley, I. Rashid, E. Michaelsson, E. L. Lindstedt, K. D. Croft, A. J. Kettle, G. J. Maghzal, R. Stocker, Inhibition of MPO (Myeloperoxidase) attenuates endothelial dysfunction in mouse models of vascular inflammation and atherosclerosis. *Arterioscler. Thromb. Vasc. Biol.* **39**, 1448–1457 (2019).
44. A. Johansson-Percival, Z. J. Li, D. D. Lakhiani, B. He, X. Wang, J. Hamzah, R. Ganss, Intratumoral LIGHT restores pericyte contractile properties and vessel integrity. *Cell Rep.* **13**, 2687–2698 (2015).
45. J. Wang, N. Niu, S. Xu, Z. G. Jin, A simple protocol for isolating mouse lung endothelial cells. *Sci. Rep.* **9**, 1458 (2019).
46. A. Boroujerdi, U. Tigges, J. V. Welsler-Alves, R. Milner, Isolation and culture of primary pericytes from mouse brain. *Methods Mol. Biol.* **1135**, 383–392 (2014).
47. Q. P. Su, Z. W. Zhao, L. Meng, M. Ding, W. Zhang, Y. Li, M. Liu, R. Li, Y. Q. Gao, X. S. Xie, Y. Sun, Superresolution imaging reveals spatiotemporal propagation of human replication foci mediated by CTCF-organized chromatin structures. *Proc. Natl. Acad. Sci. U.S.A.* **117**, 15036–15046 (2020).
48. N. S. Azahri, B. A. Di Bartolo, L. M. Khachigian, M. M. Kavurma, Sp1, acetylated histone-3 and p300 regulate TRAIL transcription: Mechanisms for PDGF-BB-mediated VSMC proliferation and migration. *J. Cell. Biochem.* **13**, 2597–2606 (2012).
49. A. J. De Micheli, J. A. Spector, O. Elemento, B. D. Cosgrove, A reference single-cell transcriptomic atlas of human skeletal muscle tissue reveals bifurcated muscle stem cell populations. *Skelet. Muscle* **10**, 19 (2020).
50. G. X. Zheng, J. M. Terry, P. Belgrader, P. Ryvkin, Z. W. Bent, R. Wilson, S. B. Ziraldo, T. D. Wheeler, G. P. McDermott, J. Zhu, M. T. Gregory, J. Shuga, L. Montesclaros, J. G. Underwood, D. A. Masquelier, S. Y. Nishimura, M. Schnell-Levin, P. W. Wyatt, C. M. Hindson, R. Bharadwaj, A. Wong, K. D. Ness, L. W. Beppu, H. J. Deeg, C. McFarland, K. R. Loeb, W. J. Valente, N. G. Ericson, E. A. Stevens, J. P. Radich, T. S. Mikkelsen, B. J. Hindson, J. H. Bielas, Massively parallel digital transcriptional profiling of single cells. *Nat. Commun.* **8**, 14049 (2017).
51. Y. Hao, S. Hao, E. Andersen-Nissen, W. M. Mauck III, S. Zheng, A. Butler, M. J. Lee, A. J. Wilk, C. Darby, M. Zager, P. Hoffman, M. Stoeciuk, E. Papalexi, E. P. Mimitou, J. Jain, A. Srivastava, T. Stuart, L. M. Fleming, B. Yeung, A. J. Rogers, J. M. McElrath, C. A. Blish, R. Gottardo, P. Smibert, R. Satija, Integrated analysis of multimodal single-cell data. *Cell* **184**, 3573–3587.e29 (2021).
52. P. L. Germain, A. Lun, C. Garcia Meixide, W. Macnair, M. D. Robinson, Doublet identification in single-cell sequencing data using scDblFinder. *F1000Res* **10**, 979 (2021).
53. T. Wu, E. Hu, S. Xu, M. Chen, P. Guo, Z. Dai, T. Feng, L. Zhou, W. Tang, L. Zhan, X. Fu, S. Liu, X. Bo, G. Yu, clusterProfiler 4.0: A universal enrichment tool for interpreting omics data. *Innovation* **2**, 100141 (2021).
54. K. Steinwede, S. Henken, J. Bohling, R. Maus, B. Ueberberg, C. Brumshagen, E. L. Brincks, T. S. Griffith, T. Welte, U. A. Maus, TNF-related apoptosis-inducing ligand (TRAIL) exerts therapeutic efficacy for the treatment of pneumococcal pneumonia in mice. *J. Exp. Med.* **209**, 1937–1952 (2012).
55. K. He, T. Wang, X. Huang, Z. Yang, Z. Wang, S. Zhang, X. Sui, J. Jiang, L. Zhao, PPP1R14B is a diagnostic prognostic marker in patients with uterine corpus endometrial carcinoma. *J. Cell. Mol. Med.* **27**, 846–863 (2023).
56. A. C. Straub, A. W. Lohman, M. Billaud, S. R. Johnstone, S. T. Dwyer, M. Y. Lee, P. S. Bortz, A. K. Best, L. Columbus, B. Gaston, B. E. Isakson, Endothelial cell expression of haemoglobin alpha regulates nitric oxide signalling. *Nature* **491**, 473–477 (2012).
57. Y. Wu, Z. Chen, G. Xie, H. Zhang, Z. Wang, J. Zhou, F. Chen, J. Li, L. Chen, H. Niu, H. Wang, RNA m(1)A methylation regulates glycolysis of cancer cells through modulating ATP5D. *Proc. Natl. Acad. Sci. U.S.A.* **119**, e2119038119 (2022).
58. J. Wang, E. Zhao, B. Geng, W. Zhang, Z. Li, Q. Liu, W. Liu, W. Zhang, W. Hou, N. Zhang, Z. Liu, B. You, P. Wu, X. Li, Downregulation of UBB potentiates SP1/VEGFA-dependent angiogenesis in clear cell renal cell carcinoma. *Oncogene* **43**, 1386–1396 (2024).
59. K. C. Chiang, S. T. Huang, R. C. Wu, S. C. Huang, T. S. Yeh, M. H. Chen, J. T. Hsu, L. W. Chen, S. F. Kuo, H. Y. Chueh, H. H. Juang, S. I. Hung, C. N. Yeh, J. S. Pang, Interferon alpha-inducible protein 27 is an oncogene and highly expressed in cholangiocarcinoma patients with poor survival. *Cancer Manag. Res.* **11**, 1893–1905 (2019).
60. L. Pan, H. Xiao, R. Liao, Q. Chen, C. Peng, Y. Zhang, T. Mu, Z. Wu, Fatty acid binding protein 5 promotes tumor angiogenesis and activates the IL6/STAT3/VEGFA pathway in hepatocellular carcinoma. *Biomed. Pharmacother.* **106**, 68–76 (2018).
61. D. D. Cheng, S. J. Li, B. Zhu, S. M. Zhou, Q. C. Yang, EEF1D overexpression promotes osteosarcoma cell proliferation by facilitating Akt-mTOR and Akt-bad signaling. *J. Exp. Clin. Cancer Res.* **37**, 50 (2018).
62. L. Yang, Z. Dong, S. Li, T. Chen, ESM1 promotes angiogenesis in colorectal cancer by activating PI3K/Akt/mTOR pathway, thus accelerating tumor progression. *Aging* **15**, 2920–2936 (2023).
63. J. Wu, F. Lu, B. Yu, W. Wang, X. Ye, The oncogenic role of SNRPB in human tumors: A pan-cancer analysis. *Front. Mol. Biosci.* **9**, 994440 (2022).
64. K. Ohashi, T. Enomoto, Y. Joki, R. Shibata, Y. Ogura, Y. Kataoka, Y. Shimizu, T. Kambara, Y. Uemura, D. Yuasa, K. Matsuo, S. Hayakawa, M. Hiramatsu-Ito, T. Murohara, N. Ouchi, Neuron-derived neurotrophic factor functions as a novel modulator that enhances endothelial cell function and revascularization processes. *J. Biol. Chem.* **289**, 14132–14144 (2014).
65. I. Dragoni, M. Mariotti, G. G. Consalez, M. R. Soria, J. A. Maier, EDF-1, a novel gene product down-regulated in human endothelial cell differentiation. *J. Biol. Chem.* **273**, 31119–31124 (1998).
66. A. Buhler, S. Berger, F. Bengsch, G. Martin, H. Han, S. Vierkotten, A. Pielen, D. Boehringer, G. Schlunck, S. Fauser, H. T. Agostini, T. Reinheckel, A. Stahl, Cathepsin proteases promote angiogenic sprouting and laser-induced choroidal neovascularisation in mice. *Exp. Eye Res.* **115**, 73–78 (2013).
67. M. Kamal, D. L. Holliday, E. E. Morrison, V. Speirs, C. Toomes, S. M. Bell, Loss of CSMD1 expression disrupts mammary duct formation while enhancing proliferation, migration and invasion. *Oncol. Rep.* **38**, 283–292 (2017).
68. P. Li, C. M. Halabi, R. Stewart, A. Butler, B. Brown, X. Xia, C. Santi, S. England, J. Ferreira, R. P. Mecham, L. Salkoff, Sodium-activated potassium channels moderate excitability in vascular smooth muscle. *J. Physiol.* **597**, 5093–5108 (2019).
69. D. Pensold, G. Zimmer, Single-cell transcriptomics reveals regulators of neuronal migration and maturation during brain development. *J. Exp. Neurosci.* **12**, 1179069518760783 (2018).
70. Y. Y. Cheng, C. M. Wright, M. B. Kirschner, M. Williams, K. H. Sarun, V. Sytnyk, I. Leshchynska, J. J. Edelman, M. P. Vallely, B. C. McCaughan, S. Klebe, N. van Zandwijk, R. C. Lin, G. Reid, KCa1.1, a calcium-activated potassium channel subunit alpha 1, is targeted by miR-17-5p and modulates cell migration in malignant pleural mesothelioma. *Mol. Cancer* **15**, 44 (2016).
71. S. Elbitar, M. Renard, P. Arnaud, N. Hanna, M. P. Jacob, D. C. Guo, K. Tsutsui, M. S. Gross, K. Kessler, L. Tosolini, V. Dattilo, S. Dupont, J. Jonquet, M. Langeois, L. Benarroch, M. Aubart, Y. Ghaleb, Y. A. Khalil, M. Varret, P. El Khoury, B. Ho-Tin-Noe, Y. Alembik, S. Gaertner, B. Isidor, L. Gouya, O. Milleron, K. Sekiguchi, D. Milewicz, J. De Backer, C. Le Goff, J. B. Michel, G. Jondeau, L. Y. Sakai, C. Boileau, M. Abifadel, Pathogenic variants in THSD4, encoding the ADAMTS-like 6 protein, predispose to inherited thoracic aortic aneurysm. *Genet. Med.* **23**, 111–122 (2021).
72. Y. Li, M. Xiao, F. Guo, The role of Sox6 and Netrin-1 in ovarian cancer cell growth, invasiveness, and angiogenesis. *Tumour Biol.* **39**, 1010428317705508 (2017).
73. W. Du, L. Huang, X. Tang, J. Li, X. Li, Ephrin-A5 is involved in retinal neovascularization in a mouse model of oxygen-induced retinopathy. *Biomed. Res. Int.* **2020**, 7161027 (2020).
74. C. L. Speyer, A. H. Hachem, A. A. Assi, J. S. Johnson, J. A. DeVries, D. H. Gorski, Metabotropic glutamate receptor-1 as a novel target for the antiangiogenic treatment of breast cancer. *PLOS ONE* **9**, e88830 (2014).
75. D. Zhu, A. Shen, Y. Wang, X. Gu, J. Gu, Developmental regulation of beta-1,3-galactosyltransferase-1 gene expression in mouse brain. *FEBS Lett.* **538**, 163–167 (2003).
76. L. Wang, E. R. Hauser, S. H. Shah, D. Seo, P. Sivashanmugam, S. T. Exum, S. G. Gregory, C. B. Granger, J. L. Haines, C. J. Jones, D. Crossman, C. Haynes, W. E. Kraus, N. J. Freedman, M. A. Pericak-Vance, P. J. Goldschmidt-Clermont, J. M. Vance, Polymorphisms of the tumor suppressor gene LSAMP are associated with left main coronary artery disease. *Ann. Hum. Genet.* **72**, 443–453 (2008).
77. M. Hiwatari, M. Seki, R. Matsuno, K. Yoshida, T. Nagasawa, A. Sato-Otsubo, S. Yamamoto, M. Kato, K. Watanabe, M. Sekiguchi, S. Miyano, S. Ogawa, J. Takita, Novel TENM3-ALK fusion is an alternate mechanism for ALK activation in neuroblastoma. *Oncogene* **41**, 2789–2797 (2022).
78. L. A. Fatima, R. S. Campello, R. S. Santos, H. S. Freitas, A. P. Frank, U. F. Machado, D. J. Clegg, Estrogen receptor 1 (ESR1) regulates VEGFA in adipose tissue. *Sci. Rep.* **7**, 16716 (2017).
79. P. Andrikopoulos, A. Baba, T. Matsuda, M. B. A. Djamgoz, M. M. Yaqoob, S. A. Eccles, Ca²⁺ influx through reverse mode Na⁺/Ca²⁺ exchange is critical for vascular endothelial growth factor-mediated extracellular signal-regulated kinase (ERK) 1/2 activation and angiogenic functions of human endothelial cells. *J. Biol. Chem.* **286**, 37919–37931 (2011).
80. B. Chakravarti, J. Yang, K. E. Ahlers-Dannen, Z. Luo, H. A. Flaherty, D. K. Meyerholz, M. E. Anderson, R. A. Fisher, Essentiality of regulator of G protein signaling 6 and oxidized Ca²⁺/calmodulin-dependent protein kinase II in notch signaling and cardiovascular development. *J. Am. Heart Assoc.* **6**, e007038 (2017).
81. T. C. S. T. Keller, C. Lechaue, A. S. Keller, G. B. Broseghini-Filho, J. T. Butcher, H. R. A. Page, A. Islam, Z. Y. Tan, L. J. DeLalio, S. Brooks, P. Sharma, K. Hong, W. Xu, A. S. Padilha, C. A. Ruddiman, A. K. Best, E. Macal, D. B. Kim-Shapiro, G. Christ, Z. Yan, M. M. Cortese-Krott, K. Ricart, R. Patel, T. P. Bender, S. K. Sonkusare, M. J. Weiss, H. Ackerman, L. Columbus, B. E. Isakson, Endothelial alpha globin is a nitrite reductase. *Nat. Commun.* **13**, 6405 (2022).
82. T. Tsukui, K. H. Sun, J. B. Wetter, J. R. Wilson-Kanamori, L. A. Hazelwood, N. C. Henderson, T. S. Adams, J. C. Schupp, S. D. Poli, I. O. Rosas, N. Kaminski, M. A. Matthey, P. J. Wolters, D. Sheppard, Collagen-producing lung cell atlas identifies multiple subsets with distinct localization and relevance to fibrosis. *Nat. Commun.* **11**, 1920 (2020).
83. A. Yamauchi, T. Sakurai, A. Kamiyoshi, Y. Ichikawa-Shindo, H. Kawate, K. Igarashi, Y. Toriyama, M. Tanaka, T. Liu, X. Xian, A. Imai, L. Zhai, S. Owa, T. Arai, T. Shindo, Functional

- differentiation of RAMP2 and RAMP3 in their regulation of the vascular system. *J. Mol. Cell. Cardiol.* **77**, 73–85 (2014).
84. Q. Zhang, P. Putheti, Q. Zhou, Q. Liu, W. Gao, Structures and biological functions of IL-13 and IL-31 receptors. *Cytokine Growth Factor Rev.* **19**, 347–356 (2008).
 85. J. G. Barcia Duran, T. Lu, S. Houghton, F. Geng, R. Schreiner, J. Xiang, S. Rafii, D. Redmond, R. Lis, Endothelial Jak3 expression enhances pro-hematopoietic angiocrine function in mice. *Commun. Biol.* **4**, 406 (2021).
 86. J. Testori, B. Schweighofer, I. Helfrich, C. Sturtzel, K. Lipnik, S. Gesierich, P. Nasarre, R. Hofer-Warbinek, M. Bilban, H. G. Augustin, E. Hofer, The VEGF-regulated transcription factor HLX controls the expression of guidance cues and negatively regulates sprouting of endothelial cells. *Blood* **117**, 2735–2744 (2011).
 87. K. Maruyama, K. Yoneda, S. Sugita, Y. Yamamoto, M. Koike, C. Peters, Y. Uchiyama, K. Nishida, CTLA-2 Alpha is a potent inhibitor of angiogenesis in murine ocular tissue. *Antioxidants* **10**, 456 (2021).
 88. C. B. McDonald, L. Buffa, T. Bar-Mag, Z. Salah, V. Bhat, D. C. Mikles, B. J. Deegan, K. L. Seldeen, A. Malhotra, M. Sudol, R. I. Aqeilan, Z. Nawaz, A. Farooq, Biophysical basis of the binding of WWOX tumor suppressor to WBP1 and WBP2 adaptors. *J. Mol. Biol.* **422**, 58–74 (2012).
 89. H. Jiang, Y. Zhao, P. Feng, Y. Liu, Sulfiredoxin-1 inhibits PDGF-BB-induced vascular smooth muscle cell proliferation and migration by enhancing the activation of Nrf2/ARE signaling. *Int. Heart J.* **63**, 113–121 (2022).
 90. G. M. Liu, X. Ji, T. C. Lu, L. W. Duan, W. Y. Jia, Y. Liu, M. L. Sun, Y. G. Luo, Comprehensive multi-omics analysis identified core molecular processes in esophageal cancer and revealed GNGT2 as a potential prognostic marker. *World J. Gastroenterol.* **25**, 6890–6901 (2019).
 91. B. Lau, O. Beine-Golovchuk, M. Kornprobst, J. Cheng, D. Kressler, B. Jady, T. Kiss, R. Beckmann, E. Hurt, Cms1 coordinates stepwise local 90S pre-ribosome assembly with timely snR83 release. *Cell Rep.* **41**, 111684 (2022).
 92. B. Messner, J. Kern, D. Wiedemann, S. Schwaiger, A. Turkcan, C. Ploner, A. Trockenbacher, K. Aumayr, N. Bonaros, G. Laufer, H. Stuppner, G. Untergasser, D. Bernhard, 5-Methoxyleoligin, a lignan from Edelweiss, stimulates CYP26B1-dependent angiogenesis in vitro and induces arteriogenesis in infarcted rat hearts in vivo. *PLOS ONE* **8**, e58342 (2013).
 93. A. L. Mayer, C. B. Higgins, M. R. Heitmeier, T. E. Kraft, X. Qian, J. R. Crowley, K. L. Hyrc, W. L. Beatty, K. E. Yarasheski, P. W. Hruz, B. J. DeBosch, SLC2A8 (GLUT8) is a mammalian trehalose transporter required for trehalose-induced autophagy. *Sci. Rep.* **6**, 38586 (2016).
- Acknowledgments:** We thank the vascular surgery team, particularly L. Beattie and L. Turner for coordinating the sample collection and assisting with ethics at the Royal Prince Alfred Hospital, Sydney, Australia. We also thank M. Murphy for technical assistance and M. Geaghan for additional quality control on the scRNA-seq data. **Funding:** This work was supported by the National Health and Medical Research Council of Australia (GNT2028501 and GNT1188218 to S.P.C. and M.M.K.; and GNT1188503 and GNT2021463 to A.R.P.), the Heart Foundation Future Leadership Fellowship (107335 to A.R.P.), and the Heart Research Institute (S.P.C. and M.M.K.). **Author contributions:** Conceptualization: S.P.C., M.S.P., J.M., I.A., R.G., R.P.H., D.A.R., S.P., M.M.K., and T.S.G. Methodology: S.P.C., M.S.P., L.B., C.P.S., R.P., J.M., Q.P.S., R.G., J.E.P., A.R.P., J.L., D.A.R., S.P., and M.M.K. Investigation: S.P.C., M.S.P., E.K., N.L., L.B., C.P.S., P.M.C., J.M., Q.P.S., J.E.P., S.P., and M.M.K. Visualization: S.P.C., M.S.P., E.K., N.L., L.B., C.P.S., A.R.P., and M.M.K. Funding acquisition: S.P.C., R.G., A.R.P., D.A.R., and M.M.K. Project administration: S.P.C., D.A.R., S.P., and M.M.K. Supervision: S.P.C., R.P.H., A.R.P., S.P., and M.M.K. Writing—original draft: S.P.C., M.S.P., E.K., L.B., C.P.S., and M.M.K. Writing—review and editing: S.P.C., M.S.P., E.K., N.L., L.B., C.P.S., M.I.D., R.P., J.M., R.G., J.E.P., R.P.H., A.R.P., T.S.G., J.L., S.J.A., and M.M.K. Resources: S.P.C., L.B., C.P.S., R.G., J.E.P., R.P.H., A.R.P., T.S.G., D.A.R., and M.M.K. Data curation: S.P.C., E.K., C.P.S., J.M., and M.M.K. Validation: S.P.C., M.S.P., E.K., N.L., L.B., C.P.S., P.M.C., M.I.D., D.A.R., and M.M.K. Formal analysis: S.P.C., M.S.P., E.K., N.L., L.B., C.P.S., M.I.D., Q.P.S., J.E.P., and M.M.K. Software: M.S.P., M.I.D., Q.P.S., J.E.P., and A.R.P. **Competing interests:** M.M.K. is an inventor on patent application PCT/AU2024/050407 submitted by the Heart Research Institute on 26 April 2024. The status of this application is pending. The other authors declare that they have no competing interests. **Data and materials availability:** All data needed to evaluate the conclusions in the paper are present in the paper and/or the Supplementary Materials. All sequencing data from this study has been submitted to the Gene Expression Omnibus (www.ncbi.nlm.nih.gov/geo/) under accession numbers GSE266788 for human and GSE242268 for mouse datasets. *Trail*^{-/-} and *Trail-R*^{-/-} mice and Conatumumab can be provided by Amgen Extramural Alliance pending scientific review and a completed material transfer agreement. Human amputated tissues can be provided by the Sydney Local Health District pending scientific review and a completed material transfer agreement.
- Submitted 4 January 2024
Accepted 28 August 2024
Published 4 October 2024
10.1126/sciadv.adn8760